

# Network-level Safety Metrics for Overall Traffic Safety Assessment: A Case Study<sup>★</sup>

Xiwen Chen<sup>a</sup>, Hao Wang<sup>a</sup>, Abolfazl Razi<sup>a,\*</sup>, Brendan Russo<sup>b</sup>, Jason Pacheco<sup>c</sup>, John Roberts<sup>d</sup>, Jeffrey Wishart<sup>e</sup>, Larry Head<sup>f</sup>

<sup>a</sup>*School of Computing, Clemson University, Clemson, SC 29631*

<sup>b</sup>*Department of Civil Engineering, Northern Arizona University, Flagstaff, AZ 86011*

<sup>c</sup>*Department of Computer Science, The University of Arizona, Tucson, AZ 85721*

<sup>d</sup>*Arizona Department of Transportation, Phoenix, AZ 85009*

<sup>e</sup>*Exponent Co, Phoenix, AZ 85721*

<sup>f</sup>*Systems and Industrial Engineering, The University of Arizona, Tucson, AZ 85027*

## Abstract

Driving safety analysis has recently witnessed unprecedented results due to advances in computation frameworks, connected vehicle technology, new generation sensors, and artificial intelligence (AI). Particularly, the recent advances performance of deep learning (DL) methods realized higher levels of safety for autonomous vehicles and empowered volume imagery processing for driving safety analysis. An important application of DL methods is extracting driving safety metrics from traffic imagery. However, the majority of current methods use safety metrics for micro-scale analysis of individual crash incidents or near-crash events, which does not provide insightful guidelines for the overall network-level traffic management. On the other hand, large-scale safety assessment efforts mainly emphasize spatial and temporal distributions of crashes, while not always revealing the safety violations that cause crashes. To bridge these two perspectives, we define a new set of network-level safety metrics for the overall safety assessment of traffic flow by processing imagery taken by roadside infrastructure sensors. An integrative analysis of the safety metrics and crash data reveals the insightful temporal and spatial correlation between the representative network-level safety metrics and the crash frequency. The analysis is performed using two video cameras in the state of Arizona along with a 5-year crash report obtained from the Arizona Department of Transportation. The results confirm that network-level safety metrics can be used by the traffic management teams to equip traffic monitoring systems with advanced AI-based risk analysis, and timely traffic flow control decisions.

**Keywords:** Deep Learning, Driving Safety Analysis, Safety Metrics, Automated Vehicles, Connected Vehicular Technologies.

## 1. Introduction

Vehicular technology has witnessed key milestones in recent years. Most cars are heavily equipped with advanced visual and radio sensors, cameras, control units, and artificial-intelligence (AI)-platforms that make driving safer and more convenient than ever. Electric vehicles (EVs) equipped with automated driving systems (ADS) have achieved higher levels of autonomy and continue to expand their territory in the global car market[1]. Crowd-sourcing and connected vehicle (CV) services have been utilized to improve the overall operation of the vehicular networks through data and model sharing. For instance, Uber Advanced Technologies Group has recently proposed a unified deep learning (DL) framework that assists automated vehicles (AVs) to map, perceive, predict, and plan sequentially so ensure safety[2]. For example, Tesla employs a cluster with 5760 A100 GPUs to conveniently train their multimodality neural network with a 1.5 petabytes dataset[3].

The use of AI platforms is not limited to car manufacturing. It indeed made revolutionary changes to traffic monitoring

and control systems, and roadside infrastructures. Particularly, web-based high-performance computing (HPC), and vehicular edge computing (VEC) servers with graphics/tensor processing units (GPU/TPUs) have made volume data aggregation and processing, more feasible than ever [4].

Despite these technological advances, driving safety still remains one of the key challenges of today's society. Statistics show that the mortality of motor-vehicle related injuries has been constant in the years 2015 to 2019 in the US [5], and the fatalities even have been increased since the pandemic started [6, 7].

This is a global issue, and about 1.3 million people die by car accidents worldwide, and millions are injured every year according to the world health organization (WHO) [8]. These statistics reveal that modern technology has not yet been fully utilized to prevent avoidable accident casualties and fatalities.

Driving safety is pursued from different perspectives by research communities, as shown in Fig. 1. New safety and warning systems are under design and development. Examples are applying eye-tracking technology to assess drivers' distraction and fatigue [9, 10], and onboard collision avoidance systems to offer safety alerts and active brake when danger is detected [11, 12, 13]. Another research direction is crash analysis, where researchers often explore the casualty of incidents based on ve-

<sup>★</sup>This material is based upon the work supported by the National Science Foundation under Grant No. 2008784 and the Arizona Commerce Authority under Institute of Automated Mobility (IAM) project.

\*Corresponding author

Email address: arazi@clemson.edu (Abolfazl Razi)

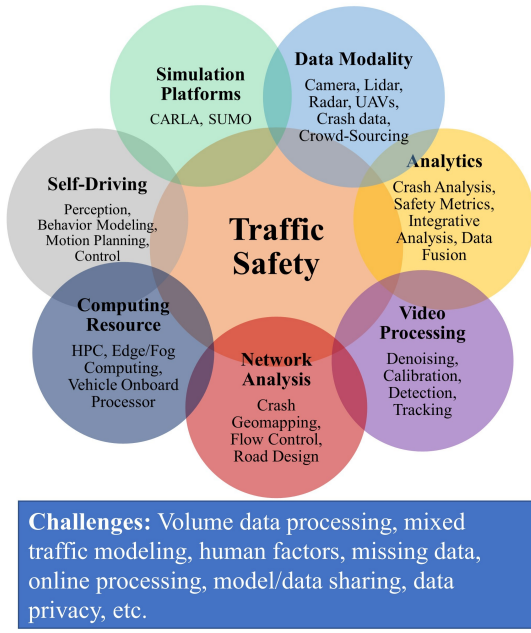


Figure 1: Different aspects, tools, opportunities, and challenges related to traffic safety.

hicle/road geometry and vehicle state ( i.e. the direction and the velocity of the vehicle). This analysis relies on a set of key parameters known as *surrogate safety metrics* (SSM) to investigate likelihood and severity of crashes under different circumstances for human-driven cars [14, 15] as well as AVs equipped with ADS [16, 17].

The community also benefits from the recent developments in image/video processing using deep learning (DL) methods with superior performance far beyond the conventional methods. DL methods have also enabled developing well-annotated volume datasets, such as the highD dataset (2018) [18] that accelerate the pace of discovery in developing even more powerful video processing methods such as YOLO series [19, 20, 21, 22] and RCNN family [23, 24, 25, 26, 27]) for object detection and tracking.

Nowadays, safety-related events such as traffic congestion, red light violation, over speeding, unauthorized-vehicle stops on the highway shoulder, etc., can be detected, interpreted, and predicted by learning-based video analysis frameworks, such as GAN-based architectures [28], query-based approaches [29], 3D convolutional Networks [30], and YOLO-family detectors [31].

To the best of our knowledge, most current methods favor the investigation of individual and independent crashes based on the extracted incident-level safety metrics and disjoint safety events. Therefore, they are not well-positioned to make relations between the crash distributions and the dynamics of the entire traffic flow.

Fig. 2 demonstrates a merge scenario, where individual safety metrics may not be capable of capturing overall safety

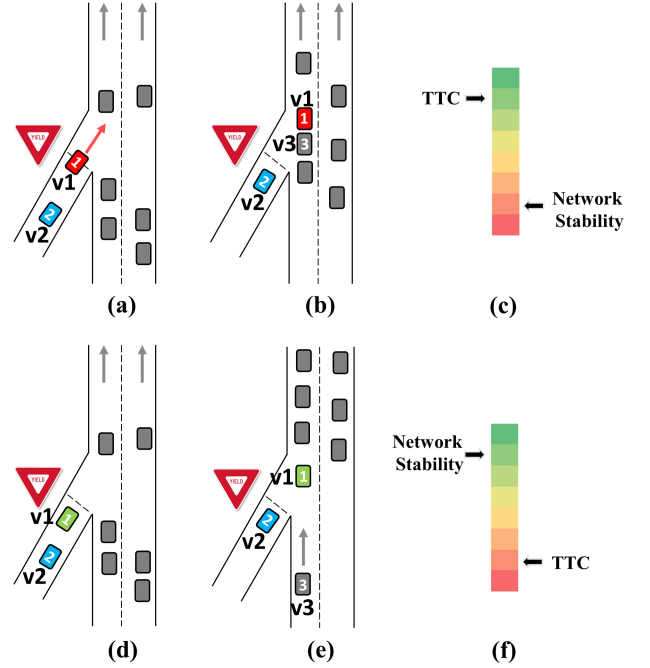


Figure 2: The individual analysis fails to interpret a merge scenario. Vehicle v1 on the entrance ramp intends to join the highway traffic. The top row (a,b) shows unsafe (aggressive) join before and after the merge. This is considered favorable by the following car (v2), since it provides a higher TTC, while disrupting the overall highway traffic stability (c). The bottom row shows the safe join by v1 after yielding the traffic flow before (d) and after the merge (e). Although this merge provides a lower TTC for the following vehicle on the ramp (v2), it is advantageous from the traffic stability point of view (f). This can be reflected in the TTC of the car following v1 after joining the highway (v3).

risks, hence can yield misleading results. Gray rectangles in this figure represent the normal traffic flow of the highway, and vehicle v1 intends to join the traffic. Figs. 2(a) and 2(b) present an aggressive merge before and after the joining epochs, while Figs. 2(c) and 2(d) show a safe merge. Let's investigate this scenario using the time-to-collision (TTC) metrics, which is one of the most commonly used safety metrics for safety analysis, especially rear-end crashes [14, 15]. Calculating TTC for the leading and following cars (v1 and v2) will favor the aggressive join, since a faster merge leaves more reaction time for the following car v2, and hence appears safer from v2's perspective. However, it causes more risk to the following vehicle on the highway after joining the traffic (v3 in Fig. 2), hence disrupting the stability of the traffic flow. This simple scenario shows how individual two-car investigations can lead to misleading results. Indeed, traffic flow can represent a complex dynamic system with many factors interacting with one another, requiring an overall network-level analysis. For instance, a traffic blockage in one intersection can influence the traffic volume (and hence the traffic safety) of alternative nearby routes.

The importance of macro-scale analysis of crash data has been recognized by some researchers [32, 33, 34, 35, 36]. However, most of these studies investigate the geo-spatial distribution of crashes and their consequences with limited insight to

finding diverse causes of crashes. More specifically, they emphasize geographical mapping of traffic properties (e.g., volume, density, congestion condition, etc.) as well as the road network topology. The high-resolution micro-level driving behaviors, such as multi-agent trajectory prediction [37], motion planning [38] have also been studied. These analyses predict crash probabilities and safety factors but they didn't try verifying their results with readily available crash reports. A brief review of these methods is provided in Section 2.

In this work, we offer a universal framework for finding meaningful correlations between representative traffic safety indicators and crash probability geo-distribution through integrative analysis of crash reports and traffic video captured by the roadside infrastructure. Our contribution is two-fold. First, we define a set of network-level safety metrics from an external observer's perspective that captures the inherent relations between local traffic flows and gauge the overall safety profile of the traffic network (Fig. 3(b)). These metrics are not claimed to be comprehensive, and are presented only to show the utility of such metrics for traffic analysis as a proof-of-concept, and can be extended to a more comprehensive list. Secondly, we provide a formal association analysis to assess the contribution of each safety metric in mediating the crash frequency. This is done by investigating the spatial and temporal correlation between the crash data points and the traffic disruption represented by the proposed safety metrics. The results of such frameworks can be used for developing online traffic advisory systems, crash explanation, risk prediction, and traffic optimization.

The overall pipeline of the proposed integrative framework is presented in Fig. 4, which includes two parallel processing modules for crash analysis and video-based safety metric extraction followed by an association analysis step.

## 2. Related Work on Network-level Analysis

Traffic analysis can be performed at different levels. In micro-level analysis, typically an individual incident is analyzed by a set of fine-resolution parameters such as the involving vehicles' geometry and motion dynamics as well as the local road and traffic flow properties, based on the sensor readings and captured imagery. A comprehensive review of micro-level analysis of crashes, DL-based driving behavior modeling, AI-platforms for driving safety enhancement have been reviewed in [39, 37, 38].

In macro-level analysis, the traffic flow is considered a dynamic network with inherent relations among network nodes. This view is adopted for network structural analysis, traffic forecasting, abnormal pattern detection, and global traffic safety analysis. For instance, [40, 41, 42, 43] consider traffic as an application of complex network theory, where the network dynamics can be represented by the collection of small-world networks [44] and random scale-free networks [45]. A small-world network is defined as a network constructed with high clustering coefficient with small average geodesics, namely the pairwise shortest path lengths. In other words, most network nodes are expected to be accessible with a low number of hops,

(e.g., logarithmic in the number of nodes). This model best fits a collection of lattice-shaped local neighborhood roads linked with a few highways.

A scale-free network is a network whose degree distribution obeys the Power-law, meaning that there exist only a few nodes with higher degrees (such as downtown or traffic hubs). Urban traffic can be modeled by such networks [40].

Some other works [46, 47, 42, 48, 49, 50, 43] analyze the network structure using complexity networks theory to evaluate, design and optimize traffic networks with sustainability and maintainability. Detecting network bottlenecks with poor connectivity and high congestion vulnerability is studied in [51, 52, 53, 54, 55, 56, 57]. It is noteworthy that some recent works [58, 59, 60] address mixed traffic taking autonomous vehicles (AVs) into consideration in their analysis.

Traffic safety can be improved by more accurate traffic forecasting, namely by predicting the future properties of the traffic flow based on current/historical features. Traffic risk modeling and prediction can provide hints and guidelines on traffic management to minimize factors that elevate the crash risk. Specifically, [61, 62] transform the road network to 2D grids and then apply CNN to predict the traffic crowd flow. The traffic flow is modeled as a diffusion process on a directed graph and deploys diffusion convolutional recurrent neural network (DCRNN) to learn the spatio-temporal features of traffic based on the historical data and road structure [63]. A method called Deep Transport is proposed in [64] which combines convolutional neural network (CNN) and recurrent neural network (RNN) architectures equipped with an attention mechanism to predict traffic volume. Recently, graph neural networks (GNNs), a class of DL networks performing inference over arbitrary graphs are proven to yield superior performance in predicting traffic-related parameters [65, 66, 67, 68, 69].

Crashes can also be viewed as severe disruptions in the network flow. Therefore, many papers have focused on abnormal network pattern detection such as inferring abnormal patterns caused by unexpected events (e.g., natural disasters, serious car accidents, traffic control) [70, 71, 72]. For instance, interpreting crashes by analyzing the frequency of irregular patterns over traffic networks is considered in the following works. The role of road factors in characterizing the severity of incidents using a logistic regression with chi-squared test is presented in [73]. Kernel density estimation (KDE) is used in [32, 33] to find the spatio-temporal patterns of traffic accidents, and rank them based on their statistical significance. Negative binomial and Poisson models are used in [34] to identify traffic factors contribute to the crash frequency. Crash prediction based on random forest (RF), gradient boosting decision tree (GBDT), and Xgboost is performed in [35]. A spatial econometric model is adopted to find associations between the road links and incidents [36].

The above-mentioned works provide insightful results for different traffic problems by network-level analysis of traffic flow and crash statistics. However, they still suffer from a few drawbacks. Some works are devoted to explaining the traffic flow and crash distributions using deep learning models. Although successful from modeling and prediction perspectives,

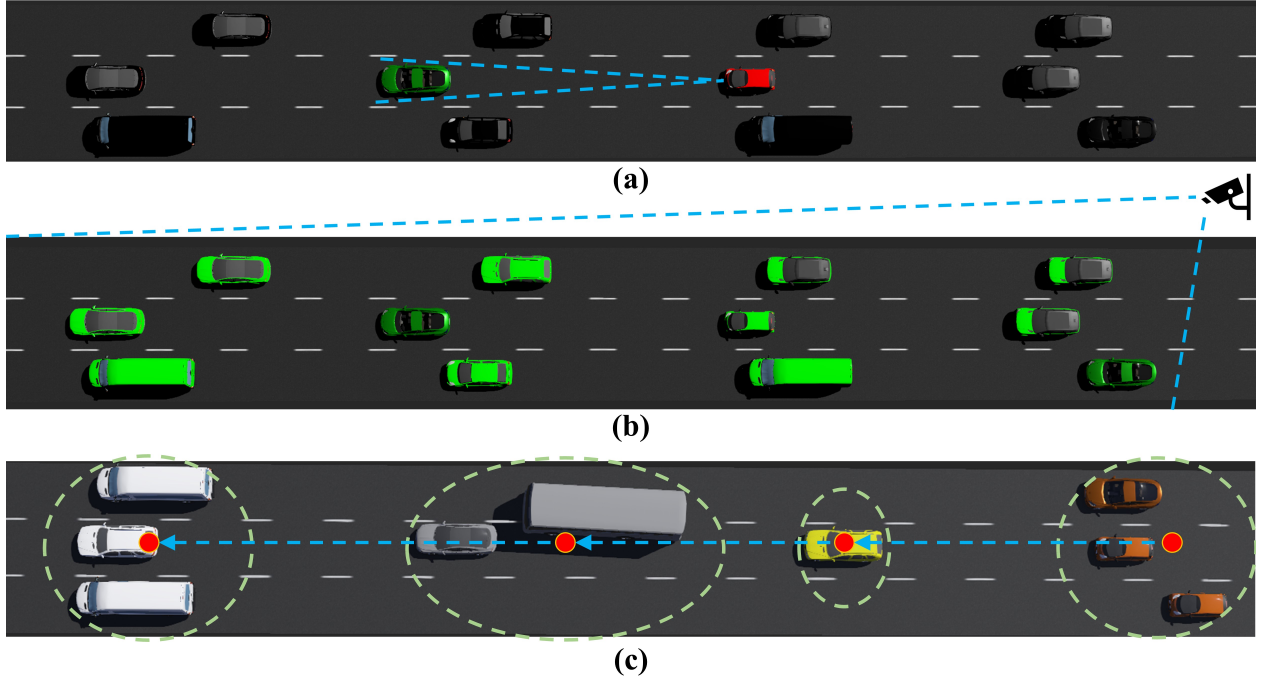


Figure 3: Different levels of traffic safety along with their regions of interest for (a) individual safety analysis from the vehicle' perspective using standard safety metrics, (b) global safety analysis from an external observer's perspective using the proposed network-level metrics, and (c) local analysis of traffic clusters.

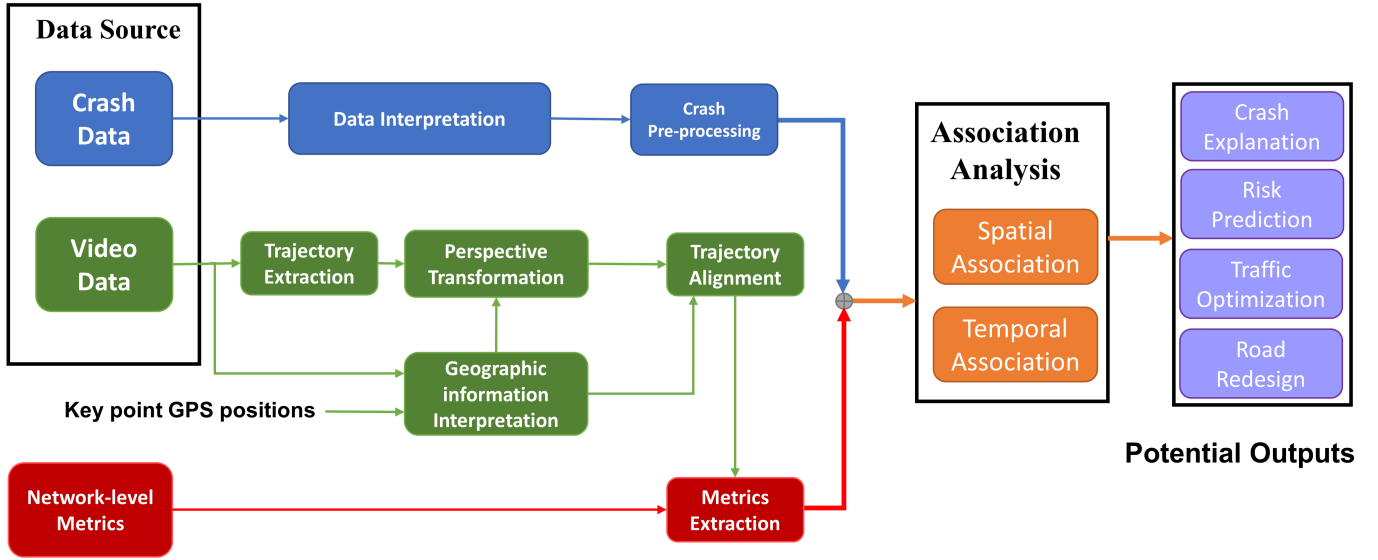


Figure 4: The proposed network-level traffic safety analysis framework includes multiple modules: (i) video processing that includes video preparation (e.g., video stabilization, noise reduction, and personal information masking), trajectory extraction, geo-mapping with perspective translation, and network-level safety metric extraction, (ii) crash analysis which includes crash temporal and spatial mapping, crash distribution (histogram), and crash type mapping (representation), and (iii) temporal and spatial association analysis.



these methods lack the interpretability and generalizeability features. Moreover, due to the difficulty of creating crash scenarios, the micro-level analysis is hardly verifiable, and most works settle with verifying the results with virtual simulators such as car learning to act (CARLA) [74] and simulation of urban mobility (SUMO) [75], ignoring the valuable information exploitable from a rich set of well-documented crash data. Furthermore, the utilized safety metrics are appropriate only for individual crash analysis, hence fail in modeling the inherent and complex relations among network nodes. In this work, we make a connection between the global analysis and deep analysis of individual incidents by introducing newly-defined network-level metrics. The integrative analysis of traffic video and crash data enables us to look for causal relations between traffic properties and crash risks and drawing general conclusions on traffic safety enhancement.

### 3. Proposed Metrics for Network-level Analysis

As stated above, conventional safety metrics are defined for scenarios where only two (or a few) vehicles are involved. A summary of popular safety metrics is provided in Appendix A, for the sake of completeness. We also introduce a taxonomy for safety metrics based on the level of access required of ADS data, when calculating these metrics for self-driving cars. Conventional safety metrics represent a micro-scale perspective to safety problems while ignoring the network-level factors that contribute to overall traffic safety. For instance, the composition of traffic (e.g., the ratio of trucks to all vehicles) can contribute to the frequency and severity of collisions. Likewise, the overall variations of car velocities on the road can reveal information about potential risk factors. In this paper, we take a small step toward developing network-level safety metrics that can be used for the overall and long-term safety assessment of traffic flow. A list of the proposed network-level safety metrics is provided in Table 1.

**Time-to-Collision-Cluster Variation (TTC-CV)** is defined to evaluate the relative velocity of car clusters that can pose safety risks. TTC is perhaps the most commonly used safety metric that evaluates the risk of read-end crash by quantifying the time of the following car colliding with the leading car if they both retain their current speeds. We develop a new metric that extends this metric to car clusters.

The idea is to cluster vehicles based on a predefined threshold and assess the relative mobility of car clusters. More specifically, we use the down-sampled version of the traffic video, e.g., at rate 1 FPS) to cluster the cars based on their pairwise distances. If  $\mathcal{S}$  is the set of cars in the current video frame, then a cluster  $C_i = \{n_j\} \subset \mathcal{S}$  is defined so that for every  $n_j \in C_i$ , there exists at least one node  $n_k \in C_i$ ,  $j \neq k$  with  $d(n_i, n_j) \leq d_C$  and likewise any car  $n_l$  satisfying  $d(n_k, n_j) \leq d_C$  for some  $n_j \in C_i$  must be a member of  $C_i$ . Here,  $d(n_i, n_j)$  is the Euclidean distance between vehicles  $n_i$  and  $n_j$ , and  $d_C$  is a predefined threshold. The clusters are non-overlapping and we have  $C_i \cap C_j = \{\}$  for all  $i \neq j$ . Then, the cluster  $C_i$  is considered as a virtual point object at the centroid of the cluster, i.e.  $l(C_i) = \sum_{n \in C_i} l(n)/|C_i|$  with velocity  $v(C_i) = \sum_{n \in C_i} v(n)/|C_i|$ . Here,  $l(n)$ ,  $v(n)$  represent

the location and velocity of node  $n$ , and,  $|C|$  is the cardinality of set  $C$  (i.e. the number of cars in cluster  $C$ ). The TTC of  $C_i$  is calculated with respect to the potential collision point with the latest leading cluster  $C_j$  moving at a lower speed  $v(C_j) \leq v(C_i)$  as follows:

$$CTTC_i = \frac{l(C_j) - l(C_i)}{v(C_i) - v(C_j)}. \quad (1)$$

For segments with crossing road segments (intersections and merging points), we use the stationary intersection point as the potential collision point when calculating cluster TTCs. Also, note that cluster TTCs are calculated using the original video with high FPS 30. The cluster TTC reduces to the regular inter-vehicle TTCs if the threshold  $d_C$  is selected close to 0, so each car becomes a cluster. Next, the coefficient of variation of cluster-level TTCs for frame  $j$ , is calculated as:

$$TTC-CV(f_j) = \frac{std(CTTC)}{mean(CTTC)} \rho_v, \quad (2)$$

as an instantaneous network-level collision risk factor for the road segment covered by video frame  $f_j$ . Here,  $N_v$  and  $N_C$  are the numbers of vehicles and clusters in the frame, and  $\rho_v = N_v/N_C$  is the average number of vehicles in each cluster used to emphasize higher risk for more crowded clusters.

**Individual Velocity Variation Rate (IVVR)** is defined as the variation of velocities for each vehicle in a specific zone or time interval. We define it as

$$IVVR = \frac{1}{N} \sum_{i=1}^N \frac{|v_i^{max} - v_i^{min}|}{v_i^{av}}, \quad (3)$$

where  $v_i^{max}$ ,  $v_i^{min}$ ,  $v_i^{av}$  are the minimum, maximum, and average velocities of vehicle  $i$ . The higher values of this metric means that on average each vehicle changes its speed more often by accelerating and decelerating. This can be due to the road profile, density of intersections and exits, traffic volume, or road conditions.

**Overall Velocity Variation Rate (OVVR)** is defined as the variation of average velocities among vehicles in a specific zone or time interval. OVVR is defined as

$$OVVR = \frac{1}{N} \sum_{i=1}^N \frac{|v_i^{av} - v^{av}|}{v^{av}}, \quad (4)$$

where  $v_i^{av}$  is the average velocity of vehicle  $i$ , and  $v^{av} = \sum_{i=1}^N v_i^{av}/N$  is the average velocity of all vehicles. Similar to IVVR, this metric can be associated with crash rate in specific highway sections.

**Over Speeding Rate (OSR)** is defined as the rate of over-

Metric	Definition	Features
TTC-CV	$TTC-CV(f_j) = \frac{std(CTTC)}{mean(CTTC)}\rho_v$	Extend the conventional TTC to cluster level; Evaluate the global risk of the traffic flow at the network-level.
IVVR	$IVVR = \frac{1}{N} \sum_{i=1}^N \frac{ v_i^{max} - v_i^{min} }{v_i^{av}}$	Reflects the instability of traffic flow by car speed variations and crash rate; Can partially offer network re-design suggestions
OVVR	$OVVR = \frac{1}{N} \sum_{i=1}^N \frac{ v_i^{av} - v^{av} }{v^{av}}$	Overall speed variation of vehicles; Defined similar to IVVR for overall traffic speed variation; Not easily affected by outliers
OSR	$OSR_i = \frac{1}{N} \sum_{i=1}^N I(v_i^{max}/v_L > Threshold_i)$	Indication of speed limit violations; Can offer suggestions for network design
TCI	$TCI = \frac{(\sum_{c=1}^C N_c)^2}{C \sum_{c=1}^C N_c^2}$ $f_c = \frac{N_c}{\sum_{c=1}^C N_c}$ $TCI = \frac{1}{2(1-2f_1f_2)}$ , two classes	Flow composition indicator; Can be associated with elevated crash risks
NTC	$NTC = \frac{\sum l_i}{N_l * L}$	Consider vehicle shape; Reflects traffic density; Can be associated with elevated crash risks
TRT	$TRT = \frac{1}{N_c} \sum_{i=1}^{N_c}  t_r(i) - t_b(i) $	A simple and reasonable way to evaluate severity of the accidents; Can also take traffic stability into consideration

Table 1: A set of proposed network-level safety metrics.

speeding vehicles as follows:

$$OSR = \frac{1}{N} \sum_{i=1}^N I(v_i^{max} > v_L), \quad (5)$$

where  $v_L$  is the speed limit, and  $I(x > y)$  is the indicator function with  $I(x > y) = 1$  for  $x > y$  and  $I(x > y) = 0$  otherwise. Speed limits are typically set based on a standardized set of national guidelines, taking into account road geometry (e.g., radii of curves, sight distance, weather conditions) and the location profile (e.g., residential versus rural areas). A high OSR, when associated with a high crash rate, may indicate the need for taking more warning and prevention measures to avoid over-speeding, noting that over-speeding can be an important contributor to crashes. On the other hand, high OSR, when it does not correlate with a high accident rate, can indicate that speed limits could be considered for potential increase without compromising traffic safety.

The aforementioned traffic metrics can be characterized by processing the roadside cameras or by crowd-sourcing and accumulating information provided by vehicles' dash cameras.

**Traffic Composition Indicator (TCI)** is defined to gauge the diversity of vehicle types in specific road sections. For instance, it is known that a higher density of trucks on the roads can correlate with the frequency and severity of road accidents; hence trucks are prohibited in some road sections in highly-populated areas [76]. This can be due to trucks' larger deceleration inertia, more frequent break failures, and lower maneuverability levels. In general, if vehicles classified into classes  $c = 1, 2, 3, \dots, C$ , then the traffic composition can be defined as

$$TCI = \frac{(\sum_{c=1}^C N_c)^2}{C \sum_{c=1}^C N_c^2}, \quad (6)$$

$$(7)$$

where  $N_c$  is the number of vehicles in class  $c$ , and the metric is defined similarly to the Jain fairness index. This metric ranges from  $1/C$  for the most unbalanced composition to 1 for an equal number of vehicles of each type. If one is interested in evaluating the rate of a specific class like trucks to all vehicles, the following metric can be used:

$$f_c = \frac{N_c}{\sum_{i=1}^C N_i}. \quad (8)$$

When classifying cars into two classes  $c = 1$  for trucks and  $c = 2$  for non-trucks, these two metrics are related as

$$TCI = \frac{1}{2(1-2f_1f_2)}. \quad (9)$$

Lower  $TCI$  values mean that most cars are of the same type with lower risks. This metric can be estimated by processing roadside videos but requires high-complexity learning methods for vehicle detection and classification.

**Normalized Traffic Density (NTC)** is defined as the density of vehicles on road sections as

$$NTC = \frac{\sum l_i}{N_l * L}, \quad (10)$$

where  $l_i$  is the length of vehicle  $n_i$ ,  $N_l$  is the number of lanes, and  $L$  is the length of the road section. We normalize the vehicle length to capture the effect of vehicle's size. This parameter can be easily extracted from roadside videos by video processing and vehicle detection. Higher NTC values are expected to be associated with higher crash rates, and may raise the request for traffic load balance strategies.

**Traffic Recovery Time (TRT)** is defined as the time required for traffic flow recovery after incidents. The system of vehicular flow can be considered as a non-equilibrium system of interact-

ing particles [77], and the instability of a flow-free state is induced by the collective effects of the increase of fluctuations. It is known that any traffic event can suddenly lead to a jamming state, and TRT reflects the time span from an event epoch to the time point the status changes to free flow. This time is expected to be much shorter than the interval between the consecutive events for flow stability. TRT can be defined as:

$$TRT = \frac{1}{N_e} \sum_{i=1}^{N_e} |t_r(i) - t_b(i)|, \quad (11)$$

where  $N_e$  is the number of events in the monitoring interval, and  $t_b(i)$  and  $t_r(i)$ , respectively, denote the event start epoch, and the flow recovery epoch for event  $i$ . This parameter can be easily obtained from roadside videos or by crowd-sourcing the position information obtained from dash cameras.

The summary of the proposed network-level safety metrics is presented in Table 1. We believe that further efforts are needed to develop a more complete list of network-level safety metrics.

## 4. Methods

### 4.1. Data acquisition

In this work, we use two camera feeds collected by the Arizona Department of Transportation (ADOT) roadside infrastructure. As presented in Table 2, each camera covers one segment of highway I-10 and records five 2-hour MP4 videos with resolution 1280x720 and FPS 30 (each video file is about 8 Gigabytes). Two exemplary covered highway segments along with the approximate camera locations are shown in Fig. 5.

### 4.2. Video preprocessing

In order to calculate safety metrics, we need to extract motion trajectories of vehicles from the video files. To this end, we integrate a tracking algorithm called *simple online and real-time tracking with deep association metric* (DeepSORT) [78] with the *you only look once* (YOLO)-v5 [22] detector to obtain trajectories of labeled objects. DeepSORT is a real-time multi-object tracking algorithm based on Kalman filtering and Hungarian algorithm, which can consider both bounding box parameters and appearance simultaneously. Known for its speed and accuracy, YOLOv5 is an advanced proposal-free detector adopted to sustain the high-quality achievement of tracking. The centroid of detected bounding boxes is used as the position of the objects. This combination offers real-time tracking (40 FPS with a GeForce RTX 2070 GPU) with acceptable accuracy (>90%). Another advantage of this approach is tracking objects even with long occlusion periods, a frequent issue in multi-vehicle tracking.

The extracted trajectories are in the pixel domain from the camera's perspective, hence the exploited distances and velocities are not proportional to real values. In order to extract safety metrics from trajectories, we translate the position information  $(u, v)$  from the 2D pixel domain into 3D GPS positions  $(x, y, z)$

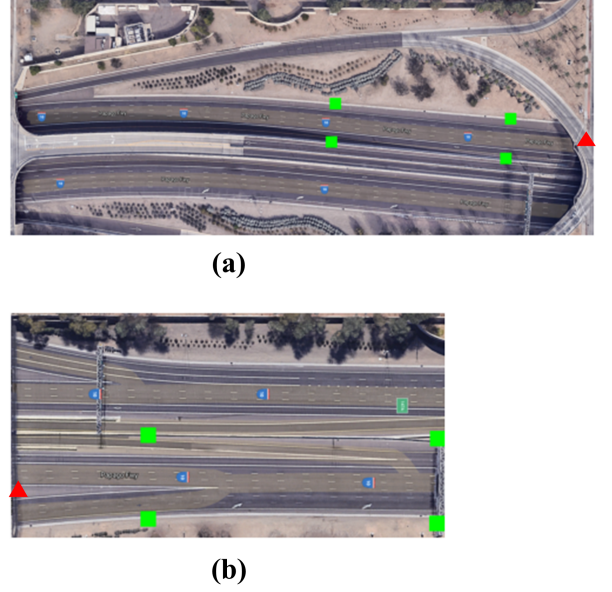


Figure 5: Selected keypoints for perspective transformation are shown by green squares, and the camera locations are by red triangles in (a) Segment #1, and (b) Segment #2.

using perspective projection. To this end, we solve the following projection equations for a set of key points with known GPS positions as shown in Fig. 5: Considering a flat surface with no elevation change, we can skip  $z$  in our calculations.

$$\begin{pmatrix} x \\ y \\ z \\ \lambda \end{pmatrix} = \begin{pmatrix} a_{11} & a_{12} & a_{13} \\ a_{21} & a_{22} & a_{23} \\ a_{31} & a_{32} & a_{33} \\ a_{41} & a_{42} & a_{43} \end{pmatrix} \begin{pmatrix} u \\ v \\ 1 \end{pmatrix}, \quad (12)$$

where,  $(x/\lambda, y/\lambda, z/\lambda)$  denotes the GPS positions of the pixel after transformation from the pixel index values  $(u, v)$  with  $\lambda$  being the scale factor. The optimal transformation coefficients  $a_{11}, \dots, a_{43}$  are obtained by applying the least squares estimation (LSE) to the set of selected keypoint pairs with known GPS positions. Under linear transformation (no camera edge distortion) four keypoints are sufficient to recover the projection matrix, but a higher accuracy can be achieved using more key points.

The obtained trajectories represent noise-like fluctuations mainly due to the drift in bounding boxes position around the object. We utilize a Savitzky–Golay (SG) filter [79] to smooth out the trajectories before performing the subsequent association analysis (Fig. 6).

### 4.3. Crash data

The crash data is also provided by ADOT, which includes crash incident details in terms of date, time, location, collision type, etc. for 5-years, from 2015 to 2019. we extract the data for covered segments and use the most dominant crash types, including the rear-end, side-swipe, and all-types, since other types like head-on, angle, and rear-to-side crashes are sparse

Table 2: The Dataset Specifications

Perspective	Resolution	FPS	Size	Raw Data Format	Analysis Data Format
External	1920*720	30	5 videos *2 views	MP4	MP4, jpg, csv

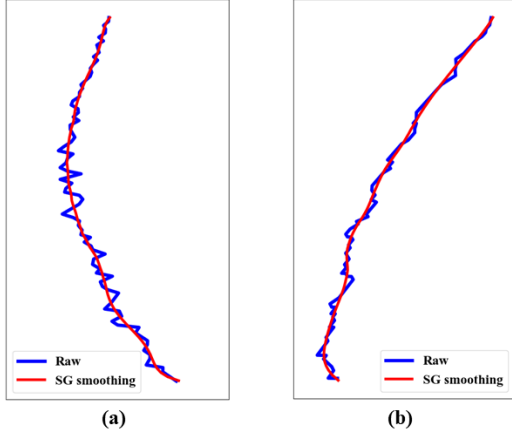


Figure 6: Some smoothed trajectories by SG filter and their original form.

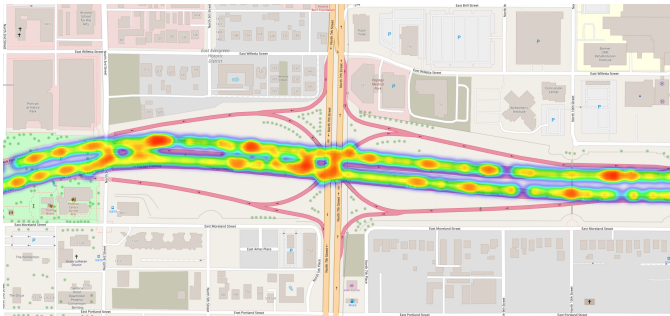


Figure 7: Geo-distribution of crash data is represented as a heatmap.

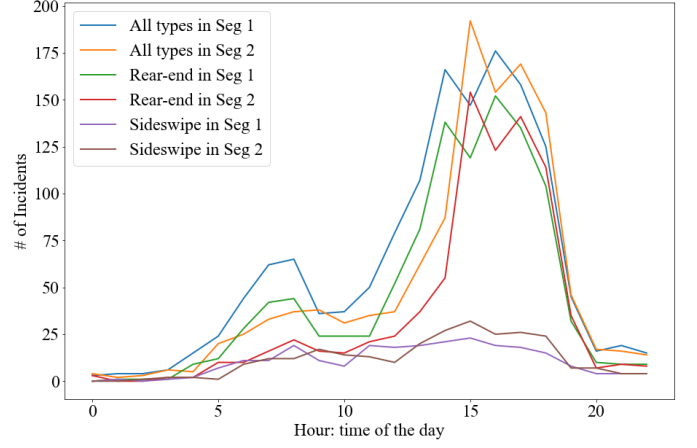


Figure 8: Crash statistics of the two segments.

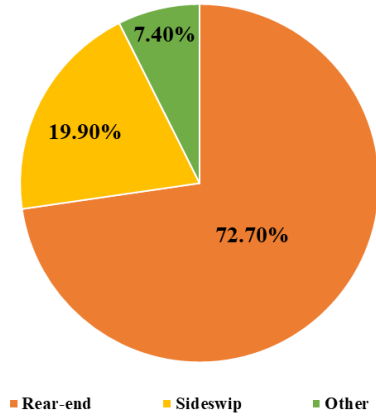


Figure 9: Ratio of crash types.

with not enough samples for association analysis. Figs. 9), 7, and 8 represent the geo-distribution of crashes and the crash statistics of the two segments, respectively.

#### 4.4. Safety metrics extraction

The utilized trajectory extraction algorithm provides vehicle IDs, and the objects' locations (in terms of bounding box corner points per video frame), and the category of each object. We model vehicles as point objects located at the center of the bounding box. The extracted trajectories, after proper handling such as perspective transformation, denoising and smoothing, and filling the missing values by linear interpolation and excluding transitional and stationary non-vehicle objects, are used to compute the proposed metrics.

This information is sufficient to calculate most of the metrics including IVVR, OVVR, and OSR metrics which are solely based on the position and velocity of the vehicles. More particularly, the position of vehicle  $n_i$  at time  $t$  is  $x_i(t) = (x_{i1}(t) + x_{i2}(t))/2$ ,  $y_i(t) = (y_{i1}(t) + y_{i2}(t))/2$ , where  $(x_{i1}(t), x_{i2}(t), y_{i1}(t), y_{i2}(t))$  represent the corner points of the corresponding bounding box at time point  $t$ . The instantaneous velocity at time  $t$  is simply the derivative of the position, i.e.  $v_i(t) = \sqrt{v_{ix}^2(t) + v_{iy}^2(t)}$ ,  $v_{ix}(t) = \alpha(x_i(t) - x_i(t - dt))/dt$ ,  $v_{iy}(t) = \alpha(y_i(t) - y_i(t - dt))/dt$  with  $\alpha$  being a scale factor into the desired metric unit and  $dt = 1/FPS$  is the time step. Higher order derivatives, and joint smoothing of the positions and velocities using methods such as Kalman filtering can also be used for higher accuracy, which we avoid in this work to keep the computational complexity at a reasonable level.

For some other metrics such as TCI and NTC, we also need the vehicle counts and types. In this work, we use only two classes of small vehicles (e.g., cars, SUVs) and large commercial vehicles (e.g., trailer trucks, busses). Since the dimensions of each object are already provided by the object detection stage (after the perspective translation and scaling), we use the object dimensions for object classification to incur minimal additional computational cost to the system. Noting the fact that the average length of personal cars and trucks is respectively about 4.5 m and 22 m [80, 81], the classification results is fairly accurate, except for the overlapping and temporarily occluded objects. For most of these objects taking the average over consecutive frames solves the transitional issues. There exist some prior work on fine-resolution vehicle classification into multiple subtypes (sedans, SUVs, truck, minivans, etc.) [82, 83, 84, 85], which we skip here in the advantage of low computational complexity for real-time monitoring systems. A summary of safety metrics is shown in Table 3.

#### 4.5. Association analysis

The goal of the association analysis is finding consistent temporal and spatial correlations between the extracted safety metrics and the frequency of different crash types.

The temporal analysis aims to verify the utility of the proposed metrics in predicting crash count in each road segment for a given time interval. The spatial analysis investigates the generalization of the identified relations to other road segments with similar conditions. Our approach to this problem is constructing a linear regression model that explains crash count in terms of extracted safety metrics. More specifically, we have

$$y_i = \mathbf{x}_i^T \beta + \varepsilon_i, \quad (13)$$

where  $\mathbf{x}_i = [x_{i1}, x_{i2}, \dots, x_{iM}]$  is the set of  $M$  extracted safety metrics for a given scenario (i.e. time interval),  $y_i$  is the crash count,  $\beta_i = [\beta_{i1}, \beta_{i2}, \dots, \beta_{iM}]$  is the vector of model parameters, and  $\varepsilon_i \sim \mathcal{N}(0, \sigma^2)$  is the zero mean model noise with variance  $\sigma^2$ . For instance, to find temporal correlations between the safety metrics and the rear-end crash types in a specific road segment, we split the time into twenty four 1-hour intervals.

Then each data sample  $\mathbf{x}_i$  represents the average of safety metrics extracted from the traffic video in a 1-hour interval (e.g., 1:00pm-2:00pm) for that specific road segment. Likewise,  $y_i$  is the frequency of rear-end crashes for all days of the data during the same time interval (1:00pm-2:00pm) that occurred in the same road segment.

Our hypothesis is that the extracted safety metrics show strong temporal and spatial correlations with the crash count. To this end, we first show that the developed models have high predictability. Then, we investigate the contribution of each individual safety metric through a formal statistical hypothesis test methods.

The residual sum of squares (RSS) for model in Eq (14) is calculated as

$$RSS = \hat{\varepsilon}^T \hat{\varepsilon} = (y - X\hat{\beta})^T (y - X\hat{\beta}), \quad (14)$$

where  $X = [\mathbf{x}_1, \mathbf{x}_2, \dots, \mathbf{x}_N]^T$  is the data matrix (each row is a data sample  $\mathbf{x}_i^T$ ), and  $\hat{\beta}$  is the estimated model parameters. Using the ordinary least square (OLS), solution of  $\hat{\beta}$  is:

$$\hat{\beta} = (X^T X)^{-1} X^T y \sim \mathcal{N}(\beta, (X^T X)^{-1} \sigma^2), \quad (15)$$

From the frequentist's perspective, the true  $\beta$  is deterministic but unknown, and we should estimate  $\hat{\beta}$  as close to  $\beta$  as possible. Since  $\varepsilon \sim \mathcal{N}(0, \sigma^2 I)$ , therefore, we have  $y \sim \mathcal{N}(X\beta, \sigma^2 I)$ . Also, we know that the best estimation of  $\beta$  by LSE is  $\hat{\beta} = (X^T X)^{-1} X^T y$ . Note that  $Y \sim \mathcal{N}(\mu, \Sigma)$  implies  $(a + BY) \sim \mathcal{N}(a + B\mu, B\Sigma B^T)$ ; therefore, we have [86]:

$$\begin{aligned} \hat{\beta} &\sim \mathcal{N}(X^T X)^{-1} X^T X\beta, (X^T X)^{-1} X^T ((X^T X)^{-1} X^T)^T \varepsilon^2) \\ \hat{\beta} &\sim \mathcal{N}(\beta, (X^T X)^{-1} X^T X (X^T X)^{-1} \varepsilon^2) \\ \hat{\beta} &\sim \mathcal{N}(\beta, (X^T X)^{-1} \varepsilon^2) \end{aligned}$$

This justifies the validity of using the subsequent statistical analysis for the relevance of normally distributed model parameters.

- **Adjusted R-squared:** This test is commonly used to validate the goodness of fit for linear regression models. Here, we use it to verify how close are the predicted crash data points using the developed model in (13) to their true values. R-squared statistics is defined as

$$R^2 = \frac{\sum(\hat{y}_i - \bar{y})^2}{\sum(y_i - \bar{y})^2}, \quad 0 \leq R^2 \leq 1, \quad (16)$$

where  $\hat{y}_i$  and  $\bar{y}$  are the estimated value and the average of the outputs  $y_i$ . Obviously, more predictors can result in stronger models in the presence of sufficient data samples. In order to account for the number of predictors and the trivial gain for using more predictors, we use Adjusted R-squared which increases when the new predictor improves

Metrics	Data Requirement	Hyperparameter
CTTC	Cluster Distance and Velocity	Potential Crash Point, Cluster min distance $d_C$
IVVR	Velocity, #of Vehicles	None
OVVR	Velocity, #of Vehicles	None
OSR	Velocity, #of Vehicles	Speed Limit
TCI	#of Vehicles in Each Class	None
NTC	#of Vehicles	Vehicle's Length*
TRT	Timestamp	None

Table 3: The summary of proposed safety metrics along with the utilized hyperparameters. \*: Vehicle's Length is calculated as 4500mm for cars and 16,000mm for trucks.

the model performance more than would be expected by chance. It is defined as:

$$R_a^2 = 1 - (1 - R^2) \frac{n-1}{n-p}, \quad (17)$$

where  $n$  is the number of samples and  $p$  is the number of predictors.

- **F-test:** This test evaluates the significance of the model by evaluating all observed variables simultaneously. More specifically, we have the following null hypothesis and alternative hypothesis:

$$\begin{aligned} H_0 : \beta_1 = \dots = \beta_k = 0, \\ H_a : \text{Not all } \beta_j \text{ are zero.} \end{aligned} \quad (18)$$

The F-test statistic can be computed by:

$$F = \frac{(TSS - RSS)/(p-1)}{RSS/(n-p)} \sim F(p-1, n-p). \quad (19)$$

If the achieved p-value is less than the given significance level  $\alpha$ , we reject the hypothesis of all model parameters being zero (irrelevant).

- **T-test:** We use this test to verify if a specific predictor of the model is active or not. The hypotheses are:

$$\begin{aligned} H_0 : \beta_j = 0, \\ H_a : \beta_j \neq 0. \end{aligned} \quad (20)$$

The t-test statistic can be computed by:

$$t_j = \frac{\hat{\beta}_j}{\text{std}(\hat{\beta}_j)} \sim t(n-p), \quad (21)$$

where,  $\text{std}(\hat{\beta}_j)$  is the standard deviation of  $\hat{\beta}_j$  computed as

$$\text{std}(\hat{\beta}_j) = \sqrt{\sigma^2(X^T X^{-1})_{jj}}. \quad (22)$$

Similarly, If the p-value is less than the given significance level  $\alpha$ , the predictor contribution is non-zero.

- **The Akaike information Criterion (AIC):** Finally, we use this test to assess the relative quality of the utilized model for a given set of data according to the fitting accuracy and the complexity of the model.

$$AIC = 2k + n \ln(RSS/n). \quad (23)$$

A lower AIC indicates a relatively better model.

## 5. Results

This section presents the results of the analysis developed in Section 4.5. The first step is generating  $6 \times 6$  one-predictor models (one model for each of the 6 safety key metrics) and 6 full-predictor models (using all safety metrics). Since we have three crash types (rear-end, wide-swipe, all-types), we build one model for each crash type for each of the two segments (seg#1 and Seg#2) resulting in a total of 6 models as shown in Table 4. We use 10 hours of video feed (9:00 am - 7: 00 pm) for two cameras for temporal analysis. We split the time into 10-min intervals, and calculate the average of developed safety metrics for each 10-min interval. This results in a total of 60 data points  $(\mathbf{x}_i, y_i)$  for each camera, where  $\mathbf{x}_i$  is the vector of extracted safety metrics and  $y_i$  is the crash count in the same interval.

The results of the full predictor-model are provided in Fig. 10 and Table 4. Plotting the predicted values of rear-end crashes based on analysing the collected traffic videos against their true values in the crash dataset for both cameras verifies the usefulness of the proposed approach of using safety metrics to predict crash rate, since most of the data samples concentrate around the unit-slope line (true value=predicted value).

A more formal statistical analysis is presented in Table 4, which further confirms the validity of the developed models. The F-value is less than  $10^{-5}$  for all scenarios which shows that



	Model Criterion			
	F P-value	R-squared	Adj. R-squared	ACI
Seg 1 All	2.65E-16	0.7902	0.7665	564.0
Seg 1 Rear-end	7.40E-17	0.8003	0.7777	553.6
Seg 1 Sideswipe	1.33E-05	0.4465	0.3839	324.5
Seg 2 All	8.59E-11	0.8896	0.8631	298.3
Seg 2 Rear-end	6.96E-11	0.8915	0.8654	290.8
Seg 2 Sideswipe	1.88E-06	0.7482	0.6878	178.7

Table 4: The all-predictor model relating the crash rate to all predictors (i.e. safety metrics). The developed models (except for the side-swipe crash model in segment 2) pass all statistical tests, showing the relevance of the introduced metrics.

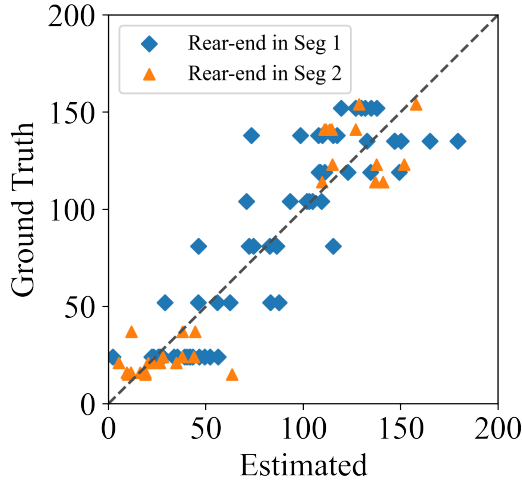


Figure 10: The scatter plot of the ground truth and the estimated value of the crash count by the full model in different segments. Each data point represents a 10-min interval.

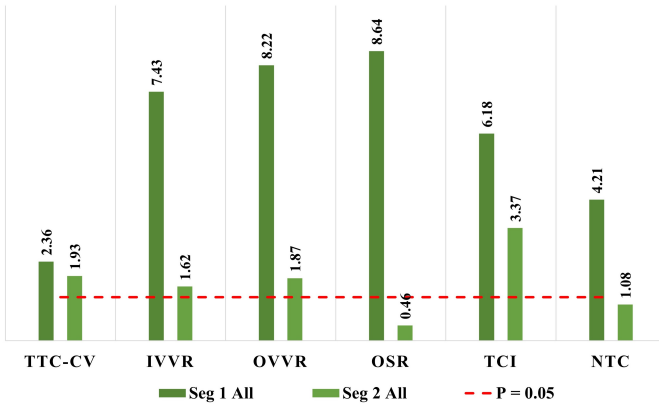


Figure 11: The illustration of P-values obtained for different metrics in association with all-types crashes using one-predictor models. The magnitude is shown as  $-\log_{10}(P)$  for visualization convenience, so the higher bars represent more significance.

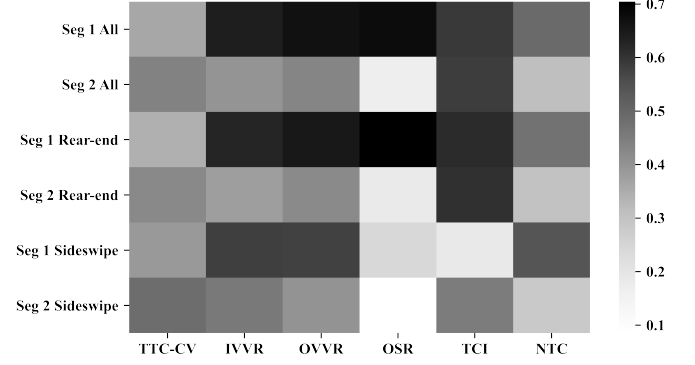


Figure 12: The significance of the Pearson correlation coefficient between different safety metrics and crash types across two segments.

the combination of all predictors (safety metrics) makes non-zero contribution to predicting crash rate, with any reasonable significance value. Also, obtaining high R-squared statistics ( $>75$ ) for All-type and Rear-end crashes across two segments suggests a strong correlation between the crash rates and safety metrics. However, side-swipe crashes seem to be more complicated in nature and potentially depend on more factors that are not well captured by the developed safety metrics, urging the need for developing a richer set of safety metrics.

To investigate the individual correlation of each safety metric, we present the results of one-predictor models in Table 5. The immediate observation is that the Pearson correlation slope sign for most metrics (except OSR) are consistent. For example, the positive slope of IVVR and OVVR shows that higher individual and overall speed variations results in a higher crash rates across the two segments. The same trend holds for TTC-CV meaning that the higher variations of TTC-CV indicate a higher chance of a crash. The negative slope of TCI indicates that the more diverse is the vehicle types (lower TCI) the most likely are crashes. The p-values of the F-test also are above 5% for most scenarios conforming the importance of the introduced safety metrics in crash risk assessment.

We also visualize the magnitude of the t-test P-value for one-predictor models in Fig. 11. The p-values are considerably lower than the significance level of 0.05, shown by a red dashed line. Fig. 12 summarizes the relations between different safety metrics and crash types in terms of Pearson correlation. The correlation is higher than 50% for most pairs (safety metric-crash type). However, one metric may not be sufficient for a reasonable prediction, as expected.

We observed that the crash rate can also be predicted even with a few extracted safety metrics, due to the inherent relation among the developed metrics. Therefore, it is advantageous to remove some of the predictors, especially for smaller datasets (like the utilized 10 hour videos per segment). We use a greedy method by starting from the full-predictor model and eliminating the predictors with lower contribution (higher p-values) as long as the overall predictability increases or remains satisfactory. Likewise, we can start combining one-predictor modes

	TTC-CV		IVVR		OVVR		OSR		TCI		NTC	
	P-value	Pearson Coefficient	P-value	Pearson Coefficient	P-value	Pearson Coefficient	P-value	Pearson Coefficient	P-value	Pearson Coefficient	P-value	Pearson Coefficient
Seg 1 All	4.38E-03	+0.3629	3.75E-08	+0.6397	6.02E-09	+0.6668	2.28E-09	-0.6801	6.61E-07	-0.5911	6.15E-05	+0.4935
Seg 1 Rear-end	7.46E-03	+0.3421	8.57E-08	+0.6265	1.52E-08	+0.6534	3.31E-10	-0.7047	1.49E-07	-0.6173	1.38E-04	+0.4726
Seg 1 Sideswipe	2.13E-03	+0.3890	1.02E-06	+0.5830	1.27E-06	+0.5787	6.11E-02	+0.2432	1.55E-01	-0.1857	8.40E-06	+0.5402
Seg 2 All	1.17E-02	+0.4401	2.42E-02	+0.3977	1.36E-02	+0.4317	3.49E-01	-0.1710	4.30E-04	-0.5856	8.35E-02	+0.3107
Seg 2 Rear-end	1.62E-02	+0.4218	3.25E-02	+0.3789	1.64E-02	+0.4212	3.12E-01	-0.1845	2.40E-04	-0.6056	8.96E-02	+0.3051
Seg 2 Sideswipe	4.88E-03	+0.4852	8.10E-03	+0.4599	2.32E-02	+0.4002	6.42E-01	-0.0853	9.31E-03	-0.4525	1.13E-01	+0.2859

Table 5: F-test results for one-predictor models  $y_i = \beta_1 x_i + \beta_0$ , where  $x_i$  is one of the proposed metrics. The slope (also as the Pearson Coefficient) indicates the linear relationship between the metric and crash. For a better generalization, the model for the same type of crash and different segments should have the same direction.

	t-Test P-value		Model Criterion				
	TTC-CV	OVVR	TCI	F P-value	R-squared	Adj. R-squared	ACI
Seg 1 All	4.16E-03	2.62E-09	2.69E-08	3.93E-15	0.7115	0.6961	577.1
Seg 2 All	5.18E-03	2.18E-06	8.11E-09	1.24E-09	0.7903	0.7678	312.9
Combined All	5.30E-12	1.15E-14	8.18E-17	1.44E-23	0.7099	0.7	896.4

Table 6: The first accepted restricted model " $TTC-CV + OVVR + TCI$ " for all type crashes analysis.

	t-Test P-value		Model Criterion				
	TTC-CV	IVVR	TCI	F P-value	R-squared	Adj. R-squared	ACI
Seg 1 All	6.24E-03	6.55E-09	9.03E-09	9.59E-15	0.7021	0.6862	579.1
Seg 2 All	9.75E-03	8.24E-05	1.76E-07	4.04E-08	0.7303	0.7014	320.9
Combined All	1.28E-01	1.32E-08	2.82E-06	9.12E-10	0.3989	0.3784	526.7

Table 7: The second accepted restricted model " $TTC-CV + IVVR + TCI$ " for all type crashes analysis.

	t-Test P-value		F P-value	Model Criterion		
	OVVR	TCI		R-squared	Adj. R-squared	ACI
Seg 1 Rear-end	8.65E-10	8.62E-08	2.79E-14	0.6655	0.6538	584.0
Seg 2 Rear-end	7.48E-07	3.18E-08	8.97E-09	0.7214	0.7022	319.9
Combined Rear-end	1.79E-08	2.76E-10	3.89E-14	0.5004	0.4891	944.4

Table 8: The third accepted restricted model " $OVVR + TCI$ " for all type crashes analysis.

	t-Test P-value		Model Criterion				
	TTC-CV	OVVR	TCI	F P-value	R-squared	Adj. R-squared	ACI
Seg 1 Rear-end	8.35E-03	4.98E-09	4.83E-09	2.96E-15	0.7145	0.6992	569.0
Seg 2 Rear-end	7.49E-03	1.56E-06	3.09E-09	7.04E-10	0.7986	0.7770	304.6
Combined Rear-end	2.24E-12	2.40E-14	1.12E-17	4.89E-24	0.7169	0.7073	879.4

Table 9: The first accepted restricted model " $TTC-CV + OVVR + TCI$ " for Rear-end crashes analysis.

	t-Test P-value		Model Criterion				
	TTC-CV	IVVR	TCI	F P-value	R-squared	Adj. R-squared	ACI
Seg 1 Rear-end	1.19E-02	1.02E-08	1.56E-09	5.96E-15	0.7072	0.6915	570.5
Seg 2 Rear-end	1.40E-02	1.06E-04	1.11E-07	4.03E-08	0.7304	0.7015	313.9
Combined Rear-end	4.44E-10	1.15E-09	3.29E-16	1.89E-19	0.6397	0.6274	901.6

Table 10: The second accepted restricted model " $TTC-CV + IVVR + TCI$ " for Rear-end crashes analysis.

	t-Test P-value		Model Criterion			
	TTC-CV	IVVR	F P-value	R-squared	Adj. R-squared	ACI
Seg 1 Sidewipe	1.17E-02	5.80E-06	2.94E-07	0.4101	0.3894	320.3
Seg 2 Sidewipe	2.02E-02	3.36E-02	2.05E-03	0.3474	0.3024	201.2
Combined Sidewipe	4.93E-01	1.74E-06	1.02E-05	0.2276	0.2103	547.8

Table 11: The first accepted restricted model " $TTC-CV + IVVR$ " for Sideswipe crashes analysis.

until achieving a desired performance. We call the resulting models as restricted models. The results of this analysis are presented in Tables 6 to 11, which show much higher prediction performance can be achieved using fewer hand-picked predictors.

We also can make a few observations from these tables which require further investigations using more data samples to make strong conclusions. i) OVVR/IVVR which gauge the velocity variations can be considered as a fundamental estimator when assessing the crashes-related tasks of different types; ii) traffic composition represented by TCI shows that an unbalanced traffic flow with more diverse vehicle types increases the chance of crashes; iii) TTC-CV or cluster level analysis of TTC presents credibility in analysing the traffic safety since it participates in most of the restricted models; iv) side swipe crashes are harder to model and perhaps human factors or road geometry play more significant roles than the general traffic flow characteristics in modulating crash rates.

## 6. Conclusion

In this paper, we offered a set of network-level safety metrics to assess the overall safety characteristics of traffic flow in a given driving zone. This concept extends the popular notation of safety metrics to network-level analysis. We conjecture that the proposed safety metrics are highly correlated by crash frequency. We conducted a case study in the state of Arizona by integrative analysis of collected video files from I-10 highway and a 5-year crash reports that verify the association between safety metrics and crash frequency using formal statistical analysis. More specifically, metrics that gauge the overall speed variation of vehicles, the traffic composition and diversity of vehicles, the density of traffic volume, and also relative mobility of car clusters are highly correlated with the crash frequency (with p-values much lower than 5% for most scenarios). We also observed that rear-end crashes are easier to predict than the side-swipe crashes, perhaps due to the stronger role of road geometry and human mistakes in side-swipe accidents. The practical use of this analysis is identifying risk factors by constant monitoring of traffic flow using AI-based roadside infrastructures in order to take more efficient short-term and long-term traffic control decisions to enhance the overall driving safety on the road.

## 7. Declaration of Competing Interest

The authors declare that they have no known competing financial interests or personal relationships that could have appeared to influence the work reported in this paper.

## 8. Acknowledgment

We would like to thank the NSF and the Institute of Automated Mobility (IAM) for supporting this work. We also thank the Arizona Department of Transportation for sharing roadside infrastructure, crash reports, and other resources with us during

the performance of this project. Also, the opinions, findings, and conclusions expressed in this manuscript are those of the author's and not necessarily those of the IAM and ADOT.

## References

- [1] Iea, Global ev outlook 2021 – analysis (Apr 2021). URL <https://www.iea.org/reports/global-ev-outlook-2021>
- [2] S. Casas, A. Sadat, R. Urtasun, Mp3: A unified model to map, perceive, predict and plan, in: Proceedings of the IEEE/CVF Conference on Computer Vision and Pattern Recognition, 2021, pp. 14403–14412.
- [3] Workshop on autonomous driving. URL <http://cvpr2021.wad.vision/>
- [4] L. Liu, C. Chen, Q. Pei, S. Maharjan, Y. Zhang, Vehicular edge computing and networking: A survey, *Mobile Networks and Applications* 26 (3) (2021) 1145–1168.
- [5] Fatality facts 2019: Yearly snapshot. URL <https://www.iihs.org/topics/fatality-statistics/detail/yearly-snapshot>
- [6] 2020 fatality data show increased traffic fatalities during pandemic (Jun 2021). URL <https://www.nhtsa.gov/press-releases/2020-fatality-data-show-increased-traffic-fatalities-during-pandemic>
- [7] Usdot releases new data showing that road fatalities spiked in first half of 2021 (Oct 2021). URL <https://www.nhtsa.gov/press-releases/usdot-release-s-new-data-showing-road-fatalities-spiked-first-half-2021>
- [8] 10 facts about road safety. URL <https://www.who.int/news-room/facts-in-pictures/detail/road-safety>
- [9] J. Xu, J. Min, J. Hu, Real-time eye tracking for the assessment of driver fatigue, *Healthcare technology letters* 5 (2) (2018) 54–58.
- [10] A. S. Le, T. Suzuki, H. Aoki, Evaluating driver cognitive distraction by eye tracking: From simulator to driving, *Transportation research interdisciplinary perspectives* 4 (2020) 100087.
- [11] Y. Ba, W. Zhang, Q. Wang, R. Zhou, C. Ren, Crash prediction with behavioral and physiological features for advanced vehicle collision avoidance system, *Transportation Research Part C: Emerging Technologies* 74 (2017) 22–33.
- [12] U. Z. Abdul Hamid, H. Zamzuri, T. Yamada, M. A. Abdul Rahman, Y. Saito, P. Raksincharoensak, Modular design of artificial potential field and nonlinear model predictive control for a vehicle collision avoidance system with move blocking strategy, *Proceedings of the Institution of Mechanical Engineers, Part D: Journal of Automobile Engineering* 232 (10) (2018) 1353–1373.
- [13] How does the toyota pre-collision system work?: Toyota safety sense™. URL <https://www.mosstoyota.com/toyota-pre-collision-system/>
- [14] H. Ge, R. Xia, H. Sun, Y. Yang, M. Huang, Construction and simulation of rear-end conflicts recognition model based on improved ttc algorithm, *IEEE Access* 7 (2019) 134763–134771.
- [15] L. Dimitriou, K. Stylianou, M. A. Abdel-Aty, Assessing rear-end crash potential in urban locations based on vehicle-by-vehicle interactions, geometric characteristics and operational conditions, *Accident Analysis & Prevention* 118 (2018) 221–235.
- [16] J. Wishart, S. Como, M. Elli, B. Russo, J. Weast, N. Altekari, E. James, Y. Chen, Driving safety performance assessment metrics for ads-equipped vehicles, Tech. rep., SAE Technical Paper (2020).
- [17] C. Wang, Y. Xie, H. Huang, P. Liu, A review of surrogate safety measures and their applications in connected and automated vehicles safety modeling, *Accident Analysis & Prevention* 157 (2021) 106157.
- [18] R. Krajewski, J. Bock, L. Kloecker, L. Eckstein, The highd dataset: A drone dataset of naturalistic vehicle trajectories on german highways for validation of highly automated driving systems, in: 2018 21st International Conference on Intelligent Transportation Systems (ITSC), IEEE, 2018, pp. 2118–2125.
- [19] J. Redmon, A. Farhadi, Yolo9000: better, faster, stronger, in: Proceedings

- of the IEEE conference on computer vision and pattern recognition, 2017, pp. 7263–7271.
- [20] J. Redmon, A. Farhadi, Yolov3: An incremental improvement, arXiv preprint arXiv:1804.02767 (2018).
  - [21] A. Bochkovskiy, C.-Y. Wang, H.-Y. M. Liao, Yolov4: Optimal speed and accuracy of object detection, arXiv preprint arXiv:2004.10934 (2020).
  - [22] G. Jocher, A. Stoken, J. Borovec, NanoCode012, A. Chaurasia, TaoXie, L. Changyu, A. V. Laughing, tkianai, yxNONG, A. Hogan, lorenzomammana, AlexWang1900, J. Hajek, L. Diaconu, Marc, Y. Kwon, oleg, wanghaoyang0106, Y. Defretin, A. Lohia, ml5ah, B. Milanko, B. Fineran, D. Khromov, D. Yiwei, Doug, Durgesh, F. Ingham, ultralytics/yolov5: v5.0 - YOLOv5-P6 1280 models, AWS, Supervise.ly and YouTube integrations (Apr. 2021). doi:10.5281/zenodo.4679653. URL <https://doi.org/10.5281/zenodo.4679653>
  - [23] R. Girshick, J. Donahue, T. Darrell, J. Malik, Rich feature hierarchies for accurate object detection and semantic segmentation, in: Proceedings of the IEEE conference on computer vision and pattern recognition, 2014, pp. 580–587.
  - [24] R. Girshick, Fast r-cnn, in: Proceedings of the IEEE international conference on computer vision, 2015, pp. 1440–1448.
  - [25] S. Ren, K. He, R. Girshick, J. Sun, Faster r-cnn: Towards real-time object detection with region proposal networks, in: Advances in neural information processing systems, 2015, pp. 91–99.
  - [26] J. Dai, Y. Li, K. He, J. Sun, R-fcn: Object detection via region-based fully convolutional networks, in: Advances in neural information processing systems, 2016, pp. 379–387.
  - [27] J. Pang, K. Chen, J. Shi, H. Feng, W. Ouyang, D. Lin, Libra r-cnn: Towards balanced learning for object detection, in: Proceedings of the IEEE conference on computer vision and pattern recognition, 2019, pp. 821–830.
  - [28] K.-T. Nguyen, D.-T. Dinh, M. N. Do, M.-T. Tran, Anomaly detection in traffic surveillance videos with gan-based future frame prediction, in: Proceedings of the 2020 International Conference on Multimedia Retrieval, 2020, pp. 457–463.
  - [29] D. Y. Fu, W. Crichton, J. Hong, X. Yao, H. Zhang, A. Truong, A. Narayan, M. Agrawala, C. Ré, K. Fatahalian, Rekall: Specifying video events using compositions of spatiotemporal labels, arXiv preprint arXiv:1910.02993 (2019).
  - [30] S. Zhou, W. Shen, D. Zeng, M. Fang, Y. Wei, Z. Zhang, Spatial-temporal convolutional neural networks for anomaly detection and localization in crowded scenes, Signal Processing: Image Communication 47 (2016) 358–368.
  - [31] K. Doshi, Y. Yilmaz, Fast unsupervised anomaly detection in traffic videos, in: Proceedings of the IEEE/CVF Conference on Computer Vision and Pattern Recognition Workshops, 2020, pp. 624–625.
  - [32] H. Harirfroush, L. Bellalite, G. B. Béné, Spatial and temporal analysis of seasonal traffic accidents, American journal of traffic and transportation engineering 4 (1) (2019) 7–16.
  - [33] A. K. Al-Aamri, G. Hornby, L.-C. Zhang, A. A. Al-Maniri, S. S. Padmadas, Mapping road traffic crash hotspots using gis-based methods: A case study of muscat governorate in the sultanate of oman, Spatial Statistics 42 (2021) 100458.
  - [34] C. Wang, F. Chen, J. Cheng, W. Bo, P. Zhang, M. Hou, F. Xiao, Random-parameter multivariate negative binomial regression for modeling impacts of contributing factors on the crash frequency by crash types, Discrete Dynamics in Nature and Society 2020 (2020).
  - [35] H. Meng, X. Wang, X. Wang, Expressway crash prediction based on traffic big data, in: Proceedings of the 2018 International Conference on Signal Processing and Machine Learning, 2018, pp. 11–16.
  - [36] T. Sipos, A. Afework Mekonnen, Z. Szabó, Spatial econometric analysis of road traffic crashes, Sustainability 13 (5) (2021) 2492.
  - [37] S. Mozaffari, O. Y. Al-Jarrah, M. Dianati, P. Jennings, A. Mouzakitis, Deep learning-based vehicle behavior prediction for autonomous driving applications: A review, IEEE Transactions on Intelligent Transportation Systems (2020).
  - [38] L. Claussmann, M. Revilloud, D. Gruyer, S. Glaser, A review of motion planning for highway autonomous driving, IEEE Transactions on Intelligent Transportation Systems 21 (5) (2019) 1826–1848.
  - [39] L. Zheng, T. Sayed, F. Mannering, Modeling traffic conflicts for use in road safety analysis: A review of analytic methods and future directions, Analytic methods in accident research 29 (2021) 100142.
  - [40] J. Wu, Z. Gao, H. Sun, H. Huang, Urban transit system as a scale-free network, Modern Physics Letters B 18 (19n20) (2004) 1043–1049.
  - [41] Z. Gao, Z. Chen, Y. Liu, K. Huang, Study on the complex network characteristics of urban road system based on gis, in: Geoinformatics 2007: Geospatial Information Technology and Applications, Vol. 6754, International Society for Optics and Photonics, 2007, p. 67540N.
  - [42] S. Boccaletti, G. Bianconi, R. Criado, C. I. Del Genio, J. Gómez-Gardenes, M. Romance, I. Sendina-Nadal, Z. Wang, M. Zanin, The structure and dynamics of multilayer networks, Physics reports 544 (1) (2014) 1–122.
  - [43] C. Klinkhamer, E. Krueger, X. Zhan, F. Blumensaat, S. Ukkusuri, P. S. C. Rao, Functionally fractal urban networks: Geospatial co-location and homogeneity of infrastructure, arXiv preprint arXiv:1712.03883 (2017).
  - [44] D. J. Watts, S. H. Strogatz, Collective dynamics of ‘small-world’ networks, nature 393 (6684) (1998) 440–442.
  - [45] A.-L. Barabási, R. Albert, Emergence of scaling in random networks, science 286 (5439) (1999) 509–512.
  - [46] M. Batty, Building a science of cities, Cities 29 (2012) S9–S16.
  - [47] M. Batty, The new science of cities, MIT press, 2013.
  - [48] R. Ding, N. Ujang, H. bin Hamid, M. S. Abd Manan, Y. He, R. Li, J. Wu, Detecting the urban traffic network structure dynamics through the growth and analysis of multi-layer networks, Physica A: Statistical Mechanics and its Applications 503 (2018) 800–817.
  - [49] S. Wang, L. Zheng, D. Yu, The improved degree of urban road traffic network: A case study of xiamen, china, Physica A: Statistical Mechanics and its Applications 469 (2017) 256–264.
  - [50] Z. Ruan, C. Song, X.-h. Yang, G. Shen, Z. Liu, Empirical analysis of urban road traffic network: A case study in hangzhou city, china, Physica A: Statistical Mechanics and its Applications 527 (2019) 121287.
  - [51] G. F. Newell, A moving bottleneck, Transportation Research Part B: Methodological 32 (8) (1998) 531–537.
  - [52] M. F. Hasan, R. C. Baliban, J. A. Elia, C. A. Floudas, Modeling, simulation, and optimization of postcombustion co<sub>2</sub> capture for variable feed concentration and flow rate. 1. chemical absorption and membrane processes, Industrial & Engineering Chemistry Research 51 (48) (2012) 15642–15664.
  - [53] J. McCre, S. Moutari, A hybrid macroscopic-based model for traffic flow in road networks, European Journal of Operational Research 207 (2) (2010) 676–684.
  - [54] J. Long, Z. Gao, H. Ren, A. Lian, Urban traffic congestion propagation and bottleneck identification, Science in China Series F: Information Sciences 51 (7) (2008) 948.
  - [55] M. Nakata, A. Yamauchi, J. Tanimoto, A. Hagishima, Dilemma game structure hidden in traffic flow at a bottleneck due to a 2 into 1 lane junction, Physica A: Statistical Mechanics and its Applications 389 (23) (2010) 5353–5361.
  - [56] C. Li, W. Yue, G. Mao, Z. Xu, Congestion propagation based bottleneck identification in urban road networks, IEEE Transactions on Vehicular Technology 69 (5) (2020) 4827–4841.
  - [57] Q.-k. Qu, F.-j. Chen, X.-j. Zhou, Road traffic bottleneck analysis for expressway for safety under disaster events using blockchain machine learning, Safety science 118 (2019) 925–932.
  - [58] Q. Lu, T. Tettamanti, D. Hörcher, I. Varga, The impact of autonomous vehicles on urban traffic network capacity: an experimental analysis by microscopic traffic simulation, Transportation Letters 12 (8) (2020) 540–549.
  - [59] A. B. Parsa, R. Shabanpour, A. Mohammadian, J. Auld, T. Stephens, A data-driven approach to characterize the impact of connected and autonomous vehicles on traffic flow, Transportation Letters (2020) 1–9.
  - [60] I. Mavromatis, A. Tassi, R. J. Piechocki, M. Sooriyabandara, On urban traffic flow benefits of connected and automated vehicles, in: 2020 IEEE 91st Vehicular Technology Conference (VTC2020-Spring), IEEE, 2020, pp. 1–7.
  - [61] J. Zhang, Y. Zheng, D. Qi, R. Li, X. Yi, Dnn-based prediction model for spatio-temporal data, in: Proceedings of the 24th ACM SIGSPATIAL international conference on advances in geographic information systems, 2016, pp. 1–4.
  - [62] J. Zhang, Y. Zheng, D. Qi, Deep spatio-temporal residual networks for citywide crowd flows prediction, in: Thirty-first AAAI conference on artificial intelligence, 2017.
  - [63] Y. Li, R. Yu, C. Shahabi, Y. Liu, Diffusion convolutional recur-

- rent neural network: Data-driven traffic forecasting, arXiv preprint arXiv:1707.01926 (2017).
- [64] X. Cheng, R. Zhang, J. Zhou, W. Xu, Deeptransport: Learning spatial-temporal dependency for traffic condition forecasting, in: 2018 International Joint Conference on Neural Networks (IJCNN), IEEE, 2018, pp. 1–8.
- [65] B. Yu, H. Yin, Z. Zhu, Spatio-temporal graph convolutional networks: A deep learning framework for traffic forecasting, arXiv preprint arXiv:1709.04875 (2017).
- [66] J. J. Q. Yu, J. Gu, Real-time traffic speed estimation with graph convolutional generative autoencoder, IEEE Transactions on Intelligent Transportation Systems 20 (10) (2019) 3940–3951.
- [67] B. Yu, Y. Lee, K. Sohn, Forecasting road traffic speeds by considering area-wide spatio-temporal dependencies based on a graph convolutional neural network (gcn), Transportation research part C: emerging technologies 114 (2020) 189–204.
- [68] J. Fu, W. Zhou, Z. Chen, Bayesian spatio-temporal graph convolutional network for traffic forecasting, arXiv preprint arXiv:2010.07498 (2020).
- [69] G. Jin, Y. Cui, L. Zeng, H. Tang, Y. Feng, J. Huang, Urban ride-hailing demand prediction with multiple spatio-temporal information fusion network, Transportation Research Part C: Emerging Technologies 117 (2020) 102665.
- [70] Z. Zhang, Q. He, H. Tong, J. Gou, X. Li, Spatial-temporal traffic flow pattern identification and anomaly detection with dictionary-based compression theory in a large-scale urban network, Transportation Research Part C: Emerging Technologies 71 (2016) 284–302.
- [71] Z. Zhang, L. Lin, Abnormal spatial-temporal pattern analysis for niagara frontier border wait times, arXiv preprint arXiv:1711.00054 (2017).
- [72] T. Huang, C. Liu, A. Sharma, S. Sarkar, Traffic system anomaly detection using spatiotemporal pattern networks, International Journal of Prognostics and Health Management 9 (1) (2018).
- [73] I. Pugachev, Y. Kulikov, G. Markelov, N. Sheshera, Factor analysis of traffic organization and safety systems, Transportation research procedia 20 (2017) 529–535.
- [74] A. Dosovitskiy, G. Ros, F. Codevilla, A. Lopez, V. Koltun, CARLA: An open urban driving simulator, in: Proceedings of the 1st Annual Conference on Robot Learning, 2017, pp. 1–16.
- [75] Simulation of urban mobility.  
URL <https://www.eclipse.org/sumo/>
- [76] W. S. Meyers, Comparison of truck and passenger-car accident rates on limited-access facilities, Transportation Research Record 808 (1981) 48–53.
- [77] Y. Sugiyama, M. Fukui, M. Kikuchi, K. Hasebe, A. Nakayama, K. Nishinari, S.-i. Tadaki, S. Yukawa, Traffic jams without bottlenecks—experimental evidence for the physical mechanism of the formation of a jam, New journal of physics 10 (3) (2008) 033001.
- [78] N. Wojke, A. Bewley, D. Paulus, Simple online and realtime tracking with a deep association metric, in: 2017 IEEE international conference on image processing (ICIP), IEEE, 2017, pp. 3645–3649.
- [79] R. W. Schafer, What is a savitzky-golay filter? [lecture notes], IEEE Signal processing magazine 28 (4) (2011) 111–117.
- [80] study: average car size is increasing - thezebra.com.  
URL <https://www.thezebra.com/resources/driving/average-car-size/>
- [81] by the numbers - standard dimensions of a semi-truck.  
URL <https://www.summittruckgroup.com/blog/by-the-numbers---standard-dimensions-of-a-semi-truck--26281>
- [82] J. Sochor, A. Herout, J. Havel, Boxcars: 3d boxes as cnn input for improved fine-grained vehicle recognition, in: Proceedings of the IEEE conference on computer vision and pattern recognition, 2016, pp. 3006–3015.
- [83] J. Sochor, J. Špaňhel, A. Herout, Boxcars: Improving fine-grained recognition of vehicles using 3-d bounding boxes in traffic surveillance, IEEE transactions on intelligent transportation systems 20 (1) (2018) 97–108.
- [84] Z. Ma, D. Chang, J. Xie, Y. Ding, S. Wen, X. Li, Z. Si, J. Guo, Fine-grained vehicle classification with channel max pooling modified cnns, IEEE Transactions on Vehicular Technology 68 (4) (2019) 3224–3233.
- [85] X. Ke, Y. Zhang, Fine-grained vehicle type detection and recognition based on dense attention network, Neurocomputing 399 (2020) 247–257.
- [86] J. J. Faraway, Linear models with R, Chapman and Hall/CRC, 2004.
- [87] S. S. Mahmud, L. Ferreira, M. S. Hoque, A. Tavassoli, Application of proximal surrogate indicators for safety evaluation: A review of recent developments and research needs, IATSS research 41 (4) (2017) 153–163.
- [88] M. M. Minderhoud, P. H. Bovy, Extended time-to-collision measures for road traffic safety assessment, Accident Analysis & Prevention 33 (1) (2001) 89–97.
- [89] M. S. Elli, J. Wishart, S. Como, S. Dhakshinamoorthy, J. Weast, Evaluation of operational safety assessment (osa) metrics for automated vehicles in simulation, SAE Technical Paper (2021).
- [90] SAE International (In development), SAE J3237 - operational safety metrics for verification and validation (V&V) of automated driving systems (ads), Recommended Practice (2020).
- [91] D. Gettman, L. Head, Surrogate safety measures from traffic simulation models, Transportation Research Record 1840 (1) (2003) 104–115.
- [92] S. Herbel, L. Laing, C. McGovern, Highway safety improvement program (hsip) manual, US Department of Transportation, Federal Highway Administration, Office of Safety, Washington, DC (2010).
- [93] A. Hawkins, California’s self-driving car reports are imperfect, but they’re better than nothing, The Verge (2019).
- [94] A. Torday, D. Baumann, A.-G. Dumont, Indicator for microsimulation-based safety evaluation, Tech. rep. (2003).

## Appendix A. Taxonomy for Operational Safety Metrics

An essential objective of operational safety analysis from a scenario perspective, as opposed to the network-level perspective that is the focus of this paper, is to implement *operational safety assessment (OSA) metrics*, which are quantifiable measures extracted from traffic videos (or other data sources). These OSA metrics allow for a determination of the operational safety of a vehicle (AV or human-driven) to be assessed as a given scenario is navigated. Here, we review key OSA metrics that have been broadly used for operational safety analysis. It is notable that many algorithms developed for AVs utilize safety metrics for safe navigation decisions and avoiding crashes; however, we consider both self-driving and human-driven vehicles.

In this Appendix, for the sake of completeness, we review key OSA metrics that have been broadly used for operational safety analysis along with the level of access to ADS data to extract these metrics for AVs. A recent paper [87] summarizes safety metrics according to different basis (temporal, distance, and deceleration):

- i **Temporal-based indicators:** Time to Collision (TTC), Extended Time to Collision (Time Exposed Time-to-Collision(TET), Time Integrated Time-to-Collision(TIT)[88]), Modified TTC (MTTC), Crash Index (CI), Time-to-Accident (TA), Time Headway (THW), and Post-Encroachment Time (PET).
- ii **Distance-based indicators:** Potential Index for Collision with Urgent Deceleration (PICUD), Proportion of stopping Distance (PSD), Margin to Collision (MTC), Difference of Space Distance and Stopping Distance (DSS), Time Integrated DSS (TIDSS), and Unsafe Density (UD);
- iii **Deceleration-based indicators:** Deceleration Rate to Avoid a Crash (DRAC), Crash Potential Index(CPI), and Criticality Index Function (CIF).

A more recent paper [16] by the metric team of the Institute of Automated Mobility (IAM), provides a comprehensive set of

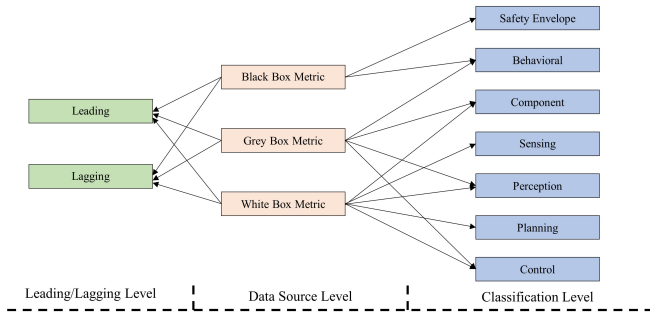


Figure A.13: Operational safety metrics taxonomy proposed by the IAM.

OSA metrics following an extensive literature review. The objective was to develop a set of metrics for both human-driven and AVs that includes existing, adapted, and novel metrics. In a follow-up paper[89], the IAM proposed a taxonomy for operational safety metrics that is explored and expanded upon here. The IAM work is also a component of an Recommended Practice standards being developed by the SAE Verification and Validation (V&V) Task Force under the On-Road Automated Driving (ORAD) Committee[90]. The taxonomy will be introduced first, and then selected OSA metrics will be discussed (including the metrics from [87] listed above).

The expanded taxonomy introduced here is shown in Figure A.13. The highest taxonomic rank in the proposed taxonomy hierarchy consists of three types that are based, essentially, on the data source, which includes the level of access required of ADS data. This access to proprietary data could be challenging, depending on the implementation of the OSA metric; it should be noted that “lighter” metrics require more cooperation with the AV developer. The three types are (example metrics are given for each, and are described in more detail later in the section):

1. **Black Box Metric:** A metric that allows measurement of data that can be obtained without requiring any access to ADS data. This could be from an on-board or off-board source. ADS data may enhance the accuracy and precision of the measurement(s). EXAMPLE: Collision incident (CI).
2. **Grey Box Metric:** A metric that allows measurement of data that can only be obtained with limited access to ADS data. EXAMPLE: ADS DDT Execution (ADE).
3. **White Box Metric:** A metric that allows measurement of data that can only be obtained with significant access to ADS data. EXAMPLE: Perception Precision (PP).

The second rank in the taxonomic hierarchy is the classification rank, which consists of the following (again, an example metric that is described later in the section is included):

1. **Safety Envelope Metric:** A metric that allows for measurement of the subject vehicle’s maintenance of a safe

boundary around itself. This includes situations that may not be within the subject vehicle’s control. EXAMPLE: Minimum Safety Envelope (MSE).

2. **Behavioral Metric:** A metric that allows for measurement of an improper behavior of the subject vehicle. EXAMPLE: Aggressive Driving (AD).
3. **Component Metric:** A metric that allows for measurement of the proper function of ADS components. EXAMPLE: Event Data Recorder Compliance (EDRC).
4. **Sensing Metric:** A metric that allows for measurement of the ability of the ADS sensors to receive adequate information from the AV environment. EXAMPLE: Camera Resolution (CR).
5. **Perception Metric:** A metric that allows for measurement of the ability of the ADS to interpret information about the AV environment obtained by the ADS sensors. EXAMPLE: Human Traffic Control Detection Error Rate (HTCDER).
6. **Planning Metric:** A metric that allows for measurement of the ability of the ADS to plan an appropriate route through the AV environment. EXAMPLE: Object Avoidance Plan Error (OAPE).
7. **Control Metric:** A metric that allows for measurement of the ability of the AV to execute the planned route devised by the ADS. EXAMPLE: Actuation Error (AE).

It is important to note that not all classification rank types link to data source rank types in the current version. For example, the Component Metric is not linked to the Black Box Metric because data at the component level is deemed to be more access to (potentially proprietary) data than is allowed for the Black Box Metric.

The third rank in the taxonomy hierarchy is the Leading/Lagging rank, which relates (in binary fashion) to either the prediction (i.e., before) of a potential operational safety outcome or report (i.e., after) of an operational safety outcome after it has occurred. Operational safety outcomes include conflicts, collisions, an ADS disengagement, or a violation of a traffic law:

1. **Leading:** An OSA identification of a potential future operational safety outcome. EXAMPLE: Any safety envelope metric.
2. **Lagging:** An OSA identification of a report of an operational safety outcome. EXAMPLE: Any traffic law violation metric.

The metrics currently being considered for inclusion in the SAE J3237 Recommended Practice<sup>1</sup> are included in Table A.12 (although the list may change)). The IAM has focused on Black

<sup>1</sup>This SAE standards document is currently in development and the operational safety metrics list could be modified, expanded, or contracted. It should



Box Metrics and Grey Box Metrics as part of the comprehensive set introduced in [87].

We also mention the approach an infrastructure-based (i.e., off-board the vehicle) observer system takes to monitor video and extract OSA metrics. The observer system also called system in the rest of this appendix for convenience, is a terrestrial or aerial monitoring system that collects traffic video for processing from an external observer's point of view. A list of these metrics, along with their brief descriptions, is presented in Table A.13.

Our main references include [91], [87] and [16].

#### Appendix A.1. Summary of Basic Operational Safety Metrics

**Maximum Speed (MaxS)**, when associated with a collision, denotes the maximum speed of the involved vehicles before the crash starts until the full stop (e.g., between time points  $t_1$  and  $t_4$  in Fig.A.14 MaxS is a simple but effective measure directly related to the severity of the collision.

**Differential Speed ( $\Delta s$ )** is defined as the relative speed between the involved vehicles. It occurs at  $t_2$  in Fig.A.14. The system needs to calculate the speed of the involved vehicles (using methods like DL-based object tracking with or without explicitly extracting the motion trajectories) to determine MaxS and *Deltas*.

**Time to Collision (TTC)** is a commonly used surrogate measure to define the time of an upcoming rear-end collision between two vehicles, if they continue their current speed ( $t_2$ - $t_3$  in Fig. A.14). The system needs to observe the relative position and calculate the relative velocity of the two involved vehicles. TTC is computed as:

$$TTC = \frac{X_L - X_F}{v_F - v_L}, \quad (A.1)$$

where  $X_i$  denotes the position,  $v_i$  denotes the velocity, and the indexes  $L$  and  $F$ , respectively, denote the leading and following vehicles. The collision occurs only if  $v_F \geq v_L$ . Usually, we have  $v_L \geq 0$  assuming that the cars move in the same direction.  $v_L \leq 0$  represents a vehicle approaching from the front. The severity of an encounter can be determined by the minimum TTC (TTCmin). Although very useful in investigating crashes, this metric has some limitations. First, TTC assumes that involved vehicles are moving at constant speeds, which ignores the potential dangers caused by acceleration or deceleration. Secondly, it assumes that the cars drive in the same direction and not appropriate for side crashes.

**Post-Encroachment Time (PET)** is defined as the time span between the encroached vehicle leaving and the other vehicle with the right-of-way arriving at the conflict point. The system

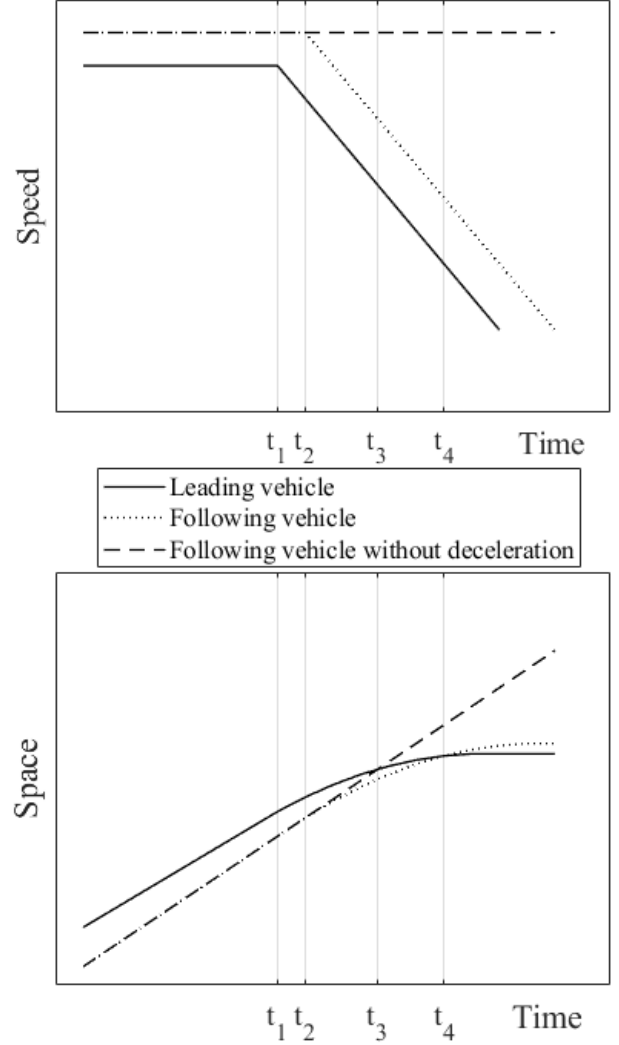


Figure A.14: The space-speed pair diagram of a rear-end collision.  $t_1$  is the time epoch the leading vehicle begins to decelerate (encroachment begin).  $t_2$  is the epoch the following vehicle begins to decelerate.  $t_1$ - $t_2$  is the reaction time of the driver of the following vehicle.  $t_3$  is the projected arrival moment of the following vehicle (under no deceleration).  $t_4$  is the actual collision moment.

be noted that the objective for the SAE J3237 document is to identify the minimum number of safety envelope metrics that will allow for an unsafe situation to be identified. Ideally, a single safety envelope metric would suffice; however, two or more safety envelope metrics may be necessary. The IAM is currently conducting research into this question of which safety envelope metrics to select, and the result may be adopted in the SAE J3237 Recommended Practice document.

Metric Name	Data Source Taxonomy	Classification Taxonomy
Minimum Safe Envelope (MSE)	Black	Safety Envelope
Proper Response (PR)	Black	Safety Envelope
Minimum Safe Distance Factor (MSDF)	Black	Safety Envelope
Time-to-Collision (TTC)	Black	Safety Envelope
Modified Time-to-Collision (MTTC)	Black	Safety Envelope
Time Headway (TH)	Black	Safety Envelope
Instantaneous Safety Metric (ISM)	Black	Safety Envelope
Collision Avoidance Capability (CAC)	Black	Safety Envelope
Minimum Safe Distance Infringement (MSDI)	Black	Safety Envelope
Post-Encroachment Time (PET)	Black	Safety Envelope
Not-at-Fault Collision Incident (NAFCI)	Black	Safety Envelope
Rear-End Collision Incident (RECI)	Black	Safety Envelope
Deceleration Rate to Avoid the Crash (DRAC)	Black	Safety Envelope
Difference of Space Distance and Stopping Distance (DSS)	Black	Safety Envelope
Maximum Speed (MaxS)	Black	Behavioral
Delta Velocity ( $\Delta V$ )	Black	Behavioral
Traffic Law Violation (TLV)	Black	Behavioral
Evasive Action (EA)	Black	Behavioral
Aggressive Driving (AD)	Black	Behavioral
Collision Incident (CI)	Black	Behavioral
ADS DDT Execution (ADE)	Grey	Control
Achieved Behavioral Competency (ABC)	Grey	Planning
Human Traffic Control Perception Error Rate (HTCDER)	Grey	Perception
Human Traffic Control Violation Rate (HTCVR)	Grey	Behavioral
Minimum Safe Distance Calculation Error (MSDCE)	Grey	Perception
Safety-Related Component Failure Perception (SRCFD)	Grey	Component
Event Data Recorder Compliance (EDRC)	Grey	Component
Perception Precision (PP)	White	Perception
Perception Rate (PDR)	White	Perception
Perception Weighted Harmonic Mean (PWHM)	White	Perception
Perception False Positive Rate (PFPR)	White	Perception
Perception False Negative Rate (PFNR)	White	Perception
Anomaly Perception Behavior (ADB)	White	Perception
Multiple Object Perception Error Rate (MODER)	White	Perception
Localization Error (LE)	White	Perception
Multiple Object Tracking Precision (MOTP)	White	Perception
Data Conflict Perception Rate (DCDR)	White	Perception
Intersection over Union (IoU)	White	Perception
Actuation Error (AE)	White	Control
Software Execution Error (SEE)	White	Component
Object Avoidance Plan Error (OAPE)	White	Planning

Table A.12: Current SAE J3237 Information Report operational safety metrics.

Metric	Definition	Features
MaxS*	$\max v$	A simple but effective measure of the severity of a collision.
$\Delta v^*$	$\Delta v$	An effective indicator of the severity of a collision.
TTC	$TTC = \frac{X_L - X_F}{v_F - v_L}$	Provides more information than PET; assumes that involved vehicles are at a constant speed; cannot reflect the severity.
PET	$PET = t_2 - t_1$	Can be easily captured and computed; suitable for assessing intersecting conflicts; only suitable for the cases of transversal trajectories; cannot reflect the severity.
Initial DR	$DR_{t=0}$	A basic indicator; cannot consider the following vehicle's acceleration/deceleration.
DRAC	$TTC = \frac{(v_F - v_L)^2}{X_L - X_F}$	No need to directly observe the deceleration rate; does not work for lateral movement
CPI*	$CPI_i = \frac{\sum_{t=t_1}^{t_2} P(DRAC_{i,t}) \geq MADR \Delta t \cdot b}{T_i}$	Considers more factors such as traffic and road conditions compared to DRAC;
PSD*	$PSD = \frac{RD}{MSD}$ $PSD = \frac{v}{2MADR}$	Works for a conflict with a single vehicle involved; rarely used for specific safety problems.
UD	$UD = \frac{\sum_{S=1}^{S_T} \sum_{V=1}^{V_T} unsafe_{TVS} \cdot d}{TL}$	Delivers more accurate information than typical micro-simulation outputs; allows comparison between simulation scenarios or links; some parameters are difficult to capture automatically; only applicable to identical trajectories.
MSE	Indicate the subject vehicle violate safety boundary of another. Safety boundary: $d_{min}^{long, same}$ (Eq.A.10) $d_{min}^{long, opp}$ (Eq.A.11) and $d_{min}^{lat}$ (Eq.A.12)	Provides how to calculate the quantified risky distances; a basis of many assessment methods.
PR	An action to recover when $d_{min}^{long}, d_{min}^{lat}$ and the safe range of $d^{lat}, d^{long}$ are violated	Adds more information beyond MSDV.
MSDF	$MSDF^{lat} = \frac{d_{min}^{lat}}{d_{max}^{lat}}$ $MSDF^{long} = \frac{d_{min}^{long}}{d_{max}^{long}}$	Can indicate the degree of defensive driving style; a higher $MSDF$ may not means higher safety.
MSDCE	$MSDCE = \sqrt{\frac{ d_{gt,min}^{long} - d_{min}^{long} }{d_{gt,min}^{long}} + \frac{ d_{gt,min}^{lat} - d_{min}^{lat} }{d_{gt,min}^{lat}}}$	Indicate the ADS ability to determine the safety distances.
CI	Indicate the subject vehicle is involved in a collision. Active when $d^{lat}$ and $d^{long}$ are equal to 0.	Capture instances of collisions as a metric; the severity of the collision can be defined by KABCO scale[92]: K(Fatal Injury), A(Incapacitating Injury), B (Non-Incapacitating Injury), C(Possible Injury), O(No Injury).
TLV	Indicate the subject vehicle that violates a traffic law	Emphasizes that an ADS vehicle must follow existing laws; exceptions are made, for example, when road closures require temporary violations of driving exclusively inside a traffic lane.
ABC	Indicate the subject vehicle can execute a specific behavior correctly.	Indicate the safety of ADS; included in the preliminary list of metrics.
ADSA	Indicate the ADS is active when executing behaviors.	Indicate the safety of ADS; included in the preliminary list of metrics; has some dispute in California[93].
HTCDER	$HTCDER = \frac{GTI - CDI}{CDI}$	One of HTC measurements; manually instructions by officers should still be considered.
HTCVR	$HTCVR = \frac{CDI - CCI}{CDI}$	One of HTC measurements; manually instructions by officers should still be considered.
AD	Indicate the maneuvers (longitudinal/lateral accelerations) of a subject vehicle exceeds specified thresholds.	The thresholds vary by jurisdiction and culture; AD is only involved the subject vehicle; implies the inherent and potential risks of natural driving behaviors; should be included when evaluating ADS.

Table A.13: Summary of operational safety metrics along with their key properties. Noting that '\*' denotes the metrics that are not selected by IAM but are basic metrics employed in other papers.

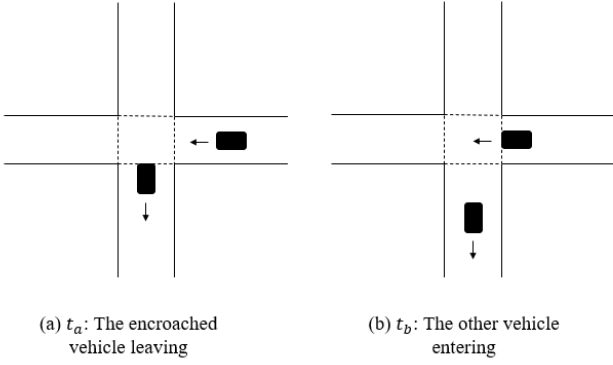


Figure A.15: The schematic diagram of PET.

needs to observe the relative time of the involved vehicles and estimate the conflict point. PET in Fig.A.15 is computed as:

$$PET = t_b - t_a, \quad (A.2)$$

where  $t_a$  and  $t_b$  represent the arrival time of the two involved vehicles. PET can be easily captured and computed by the system. However, it is suitable for intersection conflicts with transversal trajectories, but it does not fully reflect the severity of the crash.

**Initial Deceleration Rate (Initial DR)** quantifies the avoidance behavior taken by a vehicle to avoid a collision. More specifically, Initial DR (the second derivative of Curve B at time point  $t_2$  in Fig.A.14) is defined as the deceleration rate  $a_0$  at the beginning of the decelerating state. Deceleration rate is an appreciated variable to assess the potential severity of a conflict. Other variants of this metric family include Deceleration Rate to Avoid a Crash (DRAC), Crash Potential Index (CPI), and Criticality Index Function (CIF).

**Deceleration Rate to Avoid a Crash (DRAC)** is defined as the minimum deceleration rate of the following vehicle to avoid a crash to the leading vehicle. To characterize this metric, the observer system should keep track of the relative positions and the relative velocities of the two vehicles. Note that DRAC fails to evaluate lateral movements and is applicable only to scenarios where both cars are on the same lane. Mathematically, DRAC is defined as

$$DRAC = \frac{(v_F - v_L)^2}{X_L - X_F}. \quad (A.3)$$

**Crash Potential Index (CPI)** is defined as the probability of DRAC exceeding the Maximum Available Deceleration Rate (MADR) at any moment. MADR depends on the type of the vehicle as well as the environmental conditions. The system needs to calculate MADR of the target vehicles and instantaneous track time-variant deceleration to obtain the crash likelihood. CPI is defined as

$$CPI_i = \frac{\sum_{t=t_i}^{t_{f_i}} P(DRAC_{i,t}) \geq MADR \Delta t \cdot b}{T_i}, \quad (A.4)$$

where  $t_i$  and  $t_{f_i}$  are the initial and final time intervals of vehicle  $i$ , respectively,  $T_i$  denotes the total travel time of vehicle  $i$ ,  $\Delta t$  is the observation time step, and  $b$  is a binary state variable with  $b = 1$  for active state and  $b = 0$  for inactive state. Compared with DRAC, CPI considers more factors such as the traffic and road conditions, but it is not yet suitable for assessing lateral movements.

**Proportion of Stopping Distance (PSD)** is defined as the ratio of the Remaining Distance (RD) from the current position to the potential collision point to the acceptable Minimum Stopping Distance (MSD). It can be stated as

$$PSD = \frac{RD}{MSD}. \quad (A.5)$$

If MSD is considered under maximum deceleration, then PSD becomes:

$$PSD = \frac{v^2}{2MADR}. \quad (A.6)$$

PSD is an easily observable indicator and is one of the few metrics that can be used for a conflict involving a single vehicle (e.g., crashing into a stationary obstacle like a tree). PSD is defined for evasive actions and usable only for specific safety problems.

**Unsafe Density (UD)** is defined as the severity of the potential crash when the leading vehicle is within the achievable maximum DR. This metric is introduced in [94]. When multiple cars involved, this metric considers all cars in a link, while the similar metric of UnSafety (UNS) considers only two of the cars from the link to calculate the  $UNS$  of car  $v$  at time step  $s$ , denoted by  $UNS_{v,s}$ .

According to [94], the severity of a read-end crash is proportional to  $\Delta v$ , and  $v_F$ . More specifically, UNS is defined as:

$$UNS = \Delta v \cdot v_F \cdot R_d, \quad (A.7)$$

where  $R_d$  denotes the ratio between the deceleration of the leading vehicle and its maximum deceleration capacity, namely

$$R_d = \begin{cases} b/b_{max} & b < 0 \\ 0 & \text{else} \end{cases}. \quad (A.8)$$

Then, UD can be written as:

$$UD = \frac{\sum_{s=1}^{S_t} \sum_{v=1}^{V_t} UNS_{v,s} \cdot d}{TL}, \quad (A.9)$$

where  $S_t$  denotes the number of simulation steps within the aggregation period,  $V_t$  denotes the number of vehicles in the link,

$d$  denotes the time span between the two simulation steps,  $T$  denotes the aggregation period, and  $L$  denotes the section length for which the metrics are evaluated.

UD provides more accurate information than typical micro-simulation outputs and allows comparison between the simulation scenarios or links. In a transportation network, each intersection is considered as a node, and the traffic flow between the nodes is represented by a link. The two limitations of the UD parameter include (i) the difficulty of quantifying its constituent parameters and (ii) its applicability only to identical trajectories, namely when two cars move in the same direction, and the type of the potential crash is rear-end collision.

#### Appendix A.2. Operational safety metric for ADS proposed by the IAM

Here, we review part of the recently proposed metrics by the IAM [16]. These metrics are developed by a team whose leader is a co-author of this paper.

**Minimum Safe Envelope (MSE)** is defined to indicate the minimum longitudinal and lateral distances that the subject vehicle should maintain from other safety-relevant entity (often is another vehicle) for safety purposes. When the subject vehicle (subscript 1) is following behind another entity (subscript 2) and both of them are moving in the same direction. The longitudinal boundary can be defined as:

$$d_{min}^{long,same} = v_1^{long} \rho_1 + \frac{1}{2} a_{1,max,acc}^{long} \rho_1^2 + \frac{(v_1^{long} + a_{1,max,acc}^{long} \rho_1)^2}{2a_{2,min,dec}^{long}} - \frac{(v_2^{long})^2}{2a_{2,max,dec}^{long}}, \quad (A.10)$$

where  $v_i^{long/lat}$  denotes the current longitudinal/lateral velocity of vehicle  $i$ ,  $a_{i,max/min,acc/dec}^{long/lat}$  denotes the longitudinal/lateral maximum/minimum acceleration/deceleration of vehicle  $i$ , and  $\rho_i$  denotes the response time of vehicle  $i$ . When two involved vehicles are moving in opposite directions towards each other, the longitudinal boundary can be defined as:

$$d_{min}^{long,opp} = v_1^{long} \rho_1 + \frac{1}{2} a_{1,max,acc}^{long} \rho_1^2 + \frac{(v_1^{long} + a_{1,max,acc}^{long} \rho_1)^2}{2a_{1,min,dec}^{long}} + |v_2^{long}| \rho_2 + \frac{1}{2} a_{2,max,acc}^{long} \rho_2^2 + \frac{(|v_2^{long}| + a_{2,max,acc}^{long} \rho_2)^2}{2a_{2,min,dec}^{long}} \quad (A.11)$$

The lateral boundary can be defined as:

$$d_{min}^{lat} = \mu + v_1^{lat} \rho_1 + \frac{1}{2} a_{1,max,acc}^{lat} \rho_1^2 + \frac{(v_1^{lat} + a_{1,max,acc}^{lat} \rho_1)^2}{2a_{1,min,dec}^{lat}} - [v_2^{lat} \rho_2 - \frac{1}{2} a_{2,max,acc}^{lat} \rho_2^2 - \frac{(v_2^{lat} - \rho_2 a_{2,max,acc}^{lat})^2}{2a_{2,min,dec}^{lat}}], \quad (A.12)$$

where  $\mu$  is the lateral fluctuation margin. Noting that if the calculated result of  $d_{min}^{long,same}$  or  $d_{min}^{lat}$  is negative, it should be rounded up to 0. While the two boundaries are violated by the subject vehicle, MSDV is active ( $MSDV = 1$ ), meaning that an avoidable accident may occur. This metric characterizes the quantified risky distances as the basis of many assessment methods.

**Proper Response (PR)** is defined to indicate a proper action taken by the subject vehicle to recover itself when the MSE's safety boundaries ( $d_{min}^{long}$ ,  $d_{min}^{lat}$  and the safe range of  $a^{lat}$ ,  $a^{long}$ ) are violated. It adds more information beyond MSE to evaluate the behavior of the subject vehicle.

**Minimum Safe Distance Factor (MSDF)** is defined as the ratio between the current distance[s] to the calculated safe boundaries from the surrounding entity. It can be found as:

$$MSDF^{lat} = \frac{d^{lat}}{d_{min}^{lat}}, MSDF^{long} = \frac{d^{long}}{d_{min}^{long}}, \quad (A.13)$$

where  $d^{lat}$  and  $d^{long}$  denote the measured distances.  $MSDF \geq 1$  indicates the degree of defensive driving style. Note that a higher  $MSDF$  may not mean a higher safety, necessarily.

**Minimum Safe Distance Calculation Error (MSDCE)** is defined as the difference between the calculated results by ADS from the ground truth. It can be formulated as:

$$MSDCE = \sqrt{\frac{|d_{gt,min}^{long} - d_{min}^{long}|}{d_{gt,min}^{long}} + \frac{|d_{gt,min}^{lat} - d_{min}^{lat}|}{d_{gt,min}^{lat}}} \quad (A.14)$$

This metric is derived from the MSDV, which indicates the ADS ability to determine the safety distances.

**Collision Incident (CI)** is defined to indicate the subject vehicle is involved in a collision determined by the reasonably related data. CI is active when  $d^{lat}$  and  $d^{long}$  are equal to 0. Also, the severity of the collision can be defined by KABCO scale[92] with K(Fatal Injury), A(Incapacitating Injury), B (Non-Incapacitating Injury), C(Possible Injury), O(No Injury).

**Traffic Law Violation (TLV)** is defined to indicate the subject vehicle that violates a traffic law which would result in an infraction or citation. Violating these laws sets TLV active. This metric emphasizes that an ADS-vehicle must follow existing

laws, and an active TLV may lead to severe safety issues. It should be noted that exceptions to a TLV are made, for example, when road closures require temporary violations of driving exclusively inside a traffic lane.

**Achieved Behavioral Competency (ABC)** is defined to indicate the subject vehicle can execute a specific behavior correctly. This metric indicates the safety of ADS and is included in the preliminary list of ADS vehicles' metrics.

**ADS Active (ADSA)** is defined to indicate that the ADS is active when executing behaviors. This metric represents the safety of ADS and is included in the preliminary list of ADS vehicles' metrics. The metric has some dispute in California[93].

**Human Traffic Control Detection Error Rate (HTCDER)** is defined as the capability to detect instructions from a Human Traffic Control (HTC) actor correctly. It is calculated as:

$$HTCDER = \frac{GTI - CDI}{CDI}, \quad (A.15)$$

where  $GTI$  is the number of ground truth instructions, and  $CDI$  is the number of correctly detected instructions. This metric is one of the HTC measurements to evaluate the safety of the subject vehicle. Note that the manual instructions by officers should still be considered in this metric.

**Human Traffic Control Violation Rate (HTCVR)** is defined as the capability of a subject vehicle to follow the received instructions successfully. It is formulated as:

$$HTCVR = \frac{CDI - CCI}{CDI}, \quad (A.16)$$

where  $CCI$  is the number of correctly compiled instructions.

**Aggressive Driving (AD)** is defined to indicate the maneuvers (longitudinal/lateral accelerations) of a subject vehicle exceeding specified thresholds. When exceeding ( $a \geq a_T$ ), the metric is set active. The thresholds vary by jurisdiction and culture. This metric involves only the subject vehicle and implies the inherent and potential risks of natural driving behaviors. When evaluating the safety of ADS, this metric should be included.